9-2000

Photometric Variability in a Sample of 187 G and K Giants

Gregory W. Henry
Tennessee State University

Francis C. Fekel
Tennessee State University

Stephen M. Henry
Tennessee State University

Douglas S. Hall
Vanderbilt University

THE ASTROPHYSICAL JOURNAL SUPPLEMENT SERIES, 130:201–225, 2000 September

PHOTOMETRIC VARIABILITY IN A SAMPLE OF 187 G AND K GIANTS

GREGORY W. HENRY, FRANCIS C. FEKEL,[1] AND STEPHEN M. HENRY
Center of Excellence in Information Systems, Tennessee State University, 330 10th Avenue North, Nashville, TN 37203;
henry@schwab.tsuniv.edu, fekel@evans.tsuniv.edu, henrysm@galileo.tsuniv.edu

AND

DOUGLAS S. HALL
Dyer Observatory, Vanderbilt University, Nashville, TN 37235; hall@astro.dyer.vanderbilt.edu
Received 1999 December 18; accepted 2000 June 2

ABSTRACT

We have used three automatic photoelectric telescopes to obtain photometric observations of 187 G, K, and (a few) M0 field giants. We find low-amplitude photometric variability on timescales of days to weeks on both sides of the coronal dividing line (CDL) in a total of 81 or 43% of the 187 giants. About one-third of the variables have amplitudes greater than 0.01 mag in V. In our sample the percentage of variable giants is a minimum for late-G spectral classes and increases for earlier and later classes; all K5 and M0 giants are variable. We also obtained high-resolution, red wavelength spectroscopic observations of 147 of the giants, which we used to determine spectral classifications, $v \sin i$ values, and radial velocities. We acquired additional high-resolution, blue wavelength spectra of 48 of the giants, which we used to determine chromospheric emission fluxes. We analyzed the photometric and spectroscopic observations to identify the cause(s) of photometric variability in our sample of giants. We show that the light variations in the vast majority of G and K giant variables cannot be due to rotation. For giants on the cool side of the CDL, we find that the variability mechanism is radial pulsation. Thus, the variability mechanism operating in M giants extends into the K giants up to about spectral class K2. On the hot side of the CDL, the variability mechanism is most likely nonradial, g-mode pulsation.

Subject headings: stars: fundamental parameters — stars: late-type — stars: oscillations — stars: rotation — stars: spots — stars: variables: other

1. INTRODUCTION

G and K giants have often been used in variable star research as photometric comparison stars because they are bright, relatively numerous, and not expected to be intrinsically variable. Until recently, however, little observational work has been done to verify their photometric constancy. Percy (1993) conducted a search for hotter analogs of semiregular M giant variables by obtaining photometry of 49 K giants listed as named or suspected variables in The Bright Star Catalogue (Hoffleit & Jaschek 1982). He found that almost all of his program stars were constant, argued that the number of K giant variables is small, and concluded that pulsation is unlikely in K giants. Choi et al. (1995) monitored a sample of 12 G and K giants to search for photometric variability correlated with Ca II emission but found only slight variability in one of the stars. Both of those studies used small (0.25 m) automatic photoelectric telescopes (APTs) at Fairborn Observatory in Arizona that were limited to a photometric precision of about 0.01 mag. In the course of a survey to identify new chromospherically active variables with a 0.4 m APT capable of higher precision (0.004 mag), Henry, Fekel, & Hall (1995b) discovered two slowly rotating, single, K giants with photometric periods of 13.8 and 21.6 days and photometric amplitudes of 0.05 and 0.03 mag, respectively. They tentatively suggested the cause of the variations to be starspots. Using a different tactic, Hall (1995) searched the General Catalogue of Variable Stars (GCVS) (Kholopov 1985) for K giants that might be pulsating variables. He found only 17 candidates and suggested those few might have been misclassified spectroscopically, have alternative variability mechanisms, or are, in fact, constant stars.

Three recent studies have been more successful in detecting low-amplitude photometric variations in giant stars. Edmonds & Gilliland (1996) monitored the globular cluster 47 Tuc with the *Hubble Space Telescope* over a period of 38.5 hr at a photometric precision of 0.006–0.007 mag. They found 15 probable giant variables with amplitudes from 0.005–0.015 mag, estimated periods to be between 2 and 4 days, and suggested radial pulsation as the cause of the variability. In a more extensive survey, Jorissen et al. (1997) examined the onset of variability in red giant stars using the database from their Long-Term Photometry of Variables (LTPV) project; a precision of 0.002–0.003 mag was maintained over the 10 yr span of their data. They concluded from a sample of 50 G, K, and M giants that all late G and early K giants are constant at a level of $\sigma < 0.006$, where σ is the standard deviation of the observed magnitudes. For giants ranging in spectral class from K3 to mid-M, they found that the minimum variability level increased with later spectral class. Fekel & Henry (1998) presented preliminary observations of 22 variable K and early M giants, taken from the present survey, and found low-level variability throughout the K spectral class. The amplitude of variability increased from about 0.01 to 0.05 mag as the spectral type ranged from early to late K III.

With the advent of techniques for very precise relative radial velocity measurement, low-amplitude velocity variability has also been seen on different timescales in several bright, single K giants. Such variability was initially dis-

[1] Visiting Astronomer, Kitt Peak National Observatory, National Optical Astronomy Observatories, operated by the Association of Universities for Research in Astronomy, Inc., under contract with the National Science Foundation.

covered in α Boo when Smith, McMillan, & Merline (1987) found a 1.87 day period with an amplitude of 200 m s^{-1}. Hatzes & Cochran (1994a) did not confirm the 1.87 day period but did find several additional periods of less than 10 days. They concluded that the short-period variations were consistent with mode switching of radial pulsations. Hatzes & Cochran (1994b) also found β Oph to exhibit multiperiodic radial velocity variations with periods ranging from 0.26 to 142 days. That K giants have such long-term velocity variations was first shown by Walker et al. (1989), who observed five K giants, all of which had low-amplitude, radial velocity variations with timescales on the order of 1 yr. Hatzes & Cochran (1993) obtained additional velocities for three of those five K giants: α Tau, α Boo, and β Gem. They found periods of 233, 643, and 558 days, respectively, and noted that possible causes of such long-period variations include rotational modulation of surface features, nonradial pulsation, and planetary companions. Recently, the results of a couple additional radial velocity studies have been reported. Larson, Yang, & Walker (1999) acquired precise radial velocity observations of a dozen K and early M giants. They found many to have low-amplitude velocity variability with periods of several hundred days. Cummings et al. (1999) obtained high-precision radial velocities of a group of late-type evolved stars in the southern hemisphere. The velocity variations they observed for the K giants all have timescales of hundreds of days.

In this paper, we present the results of a photometric and spectroscopic survey of 187 early G to early M giants to examine further the occurrence of low-amplitude photometric variability among giant stars. In § 2, we describe the stellar sample examined in this study. Section 3 contains a description of the photometric and spectroscopic observations, and § 4 outlines the analyses of those observations. We discuss our results in § 5 and summarize our conclusions in § 6. Appendix A contains additional information and results on selected individual stars. Appendix B lists our radial velocities for the majority of the giants in our samples.

2. STELLAR SAMPLE

The 187 G, K, and (a few) early M giants in our study are divided into three samples that come from three different sources.

Sample 1 is comprised of 172 giants that served as comparison stars in an ongoing program of high-precision, differential photometry of solar-type stars with 0.75 and 0.80 m APTs (Baliunas et al. 1998; Henry 1999). Each APT acquires photometry of approximately 75 program stars with respect to three separate comparison stars. Thus, this program uses a total of several hundred comparison stars selected from random field stars surrounding each program star. The selection criteria included (1) closeness on the sky to the program star, (2) color index similar to the program star, (3) brightness (8th magnitude or brighter), (4) membership in a spectral class predominantly populated by photometrically constant stars, and (5) absence of known variability. The majority of comparison stars were chosen from spectral class F, but the existence of the earlier studies cited above on the photometric constancy of G and K giants induced us to select many late-type giants as well. Generally, only HD spectral types (i.e., no luminosity classifications) were known for the G and K stars we selected, but such types, combined with the small proper motions of the stars, suggested that they were probably giants. (The comparison stars were chosen prior to the release of the *Hipparcos* parallaxes [Perryman et al. 1997]). This group of 172 comparison stars is listed by HD number in Table 1 along with results to be described below.

TABLE 1

SAMPLE 1 GIANTS AND ANALYSIS RESULTS

HD Number (1)	Spectral Type (2)	$(B-V)_0$ (3)	M_V (mag) (4)	L ($L_\odot$) (5)	R ($R_\odot$) (6)	$v \sin i$ (km s^{-1}) (7)	Number of Seasons (8)	σ_{short} (mag) (9)	Timescale (days) (10)	$i_{predict}$ (deg) (11)	*Hipparcos* Variability Type (12)
1594.....	K0 III	0.998	1.32	33	8.2	1.3	5	0.0016			C
3346.....	M0 III	1.538	−1.54	1055	70.9	3.1	2	0.0134	11	0.5	U
3690.....	K0 III	1.129	−0.24	161	20.0	1.9	5	0.0015			D
4526.....	G8 III[a]	0.907	0.14	91	12.6		4	0.0017			
4627.....	G8 III[a]	1.055	−0.78	244	23.2		4	0.0017			
10222.....	K0 III	1.089	−0.60	216	22.4	2.4	1	0.0016			C
11326.....	K1 IV	1.074	1.20	40	9.6	1.1	4	0.0016			C
12252.....	G8 III	0.875	−0.32	136	14.9	0.4	5	0.0015			C
13611.....	G7 II–III[a]	0.851	−0.96	239	19.4		3	0.0011			C
16060.....	gG6[a]	1.025	0.73	59	11.2		5	0.0015			
16761.....	K0 III	1.005	1.21	37	8.7	1.8	1	0.0051	120	29	C
18474.....	G5 III	0.828	−0.83	210	17.8	0.6	2	0.0013			C
18832.....	K0 III	1.004	0.22	92	13.7	2.6	2	0.0016			
19845.....	K0 III	0.949	0.95	45	9.1	1.9	2	0.0013			
20791.....	G8.5 III[a]	0.942	0.88	48	9.4		3	0.0018			C
21018.....	G1 III[a]	0.768	−1.58	399	23.2		5	0.0019			D
21585.....	G1 IV:	0.756	0.57	55	8.5	4.3	2	0.0021			C
22695.....	G8 III	0.970	0.62	62	10.9	1.5	5	0.0014			C
26409.....	G8 III[a]	0.913	0.03	101	13.3		5	0.0019			
29923.....	G5 IV	0.760	2.33	11	3.8	1.3	3	0.0043	55	22	
31414.....	G8/K0 III[a]	0.918	−0.23	129	15.1		5	0.0016			
38229.....	G8 III	0.862	0.51	63	10.0	0.4	3	0.0018			C

TABLE 1—*Continued*

HD Number (1)	Spectral Type (2)	$(B-V)_0$ (3)	M_V (mag) (4)	L ($L_\odot$) (5)	R ($R_\odot$) (6)	$v \sin i$ (km s^{-1}) (7)	Number of Seasons (8)	$\sigma_{\rm short}$ (mag) (9)	Timescale (days) (10)	$i_{\rm predict}$ (deg) (11)	*Hipparcos* Variability Type (12)
40458	G1 IV:	0.854	−1.50	397	25.1	7.6	3	0.0016			
41479	K0 III	1.060	−2.40	1092	49.3	4.9	1	0.0016			
41599	K2 III	1.119	0.78	62	12.3	1.6	1	0.0015			
41790	G8 III	1.062	−1.38	427	30.9	5.1	1	0.0018			C
42596	K2 III					2.9	1	0.0018			N/A
43299	K2 III	1.200	2.18	19	7.2	1.5	1	0.0023			C
47270	K1 III[a]	1.173	−0.35	187	22.3		1	0.0020			C
47335	K0 III	0.993	0.79	54	10.4	0.4	1	0.0013			
48270	K2 III	1.128	−1.66	595	38.3	1.3	1	0.0018			C
51101	K0 III[a]	0.901	0.27	80	11.8		3	0.0018			
51833	G8 III[a]	1.253	−0.61	260	27.9		1	0.0024			
52101	K0 III[a]	0.957	−1.52	441	28.9		2	0.0020			C
53078	G8 III	0.856	0.63	56	9.4	4.4	1	0.0047	25	13	C
55576	K1 III[b]	1.084	−0.96	299	26.3		3	0.0018			C
55969	K1 III	1.070	0.36	87	14.0	0.9	1	0.0020			C
56245	K0 III	0.971	−0.54	180	18.6	3.1	3	0.0018			C
61107	G2 IV:	0.742	−0.49	144	13.6	15.1	2	0.0015			D
63838	K2 III	1.206	0.76	70	13.9	1.5	1	0.0031	15:	1.8	
64372	G7 III[a]	0.994	0.21	93	13.6		3	0.0016			C
65754	K0 III[b]	1.053	1.03	46	10.1		3	0.0019			
66285	G1 III[b]	0.682	−0.76	177	14.1		2	0.0015			
67541	K0 III					1.6	1	0.0012			N/A
68612	K2 III	1.252	0.16	129	19.6	3.0	1	0.0025			
70136	K4 III	1.330	−0.40	239	28.3	2.8	1	0.0034			
70673	K0 III[a]	0.966	0.53	67	11.4		1	0.0019			C
73108	K1 III[a]	1.160	0.08	124	17.9		6	0.0022			C
73799	K4 III	1.317	−0.57	275	30.1	3.6	1	0.0017			C
74485	G7 III	0.900	0.18	88	12.3	4.7	1	0.0030	25:	10.9	
75216	K2 III	1.102	0.14	111	16.2	2.3	1	0.0020			
76219	G8 III	0.957	−1.14	310	24.2	8.1	3	0.0018			
80811	K0 IV	0.842	2.90	7	3.3	3.0	2	0.0016			C
81872	K1 III[a]	1.000	0.69	60	11.0		2	0.0014			C
82074	G6 IV[a]	0.825	2.53	9	3.8		3	0.0015			C
84345	M0 III	1.477	−0.74	427	42.6	1.8	1	0.0202	15	0.7	U
84453	G8 III	0.929	2.15	15	5.1	0.8	3	0.0013			
86166	K2 III	1.065	0.70	63	11.9	2.6	1	0.0018			C
86873	G8 IV	0.886	2.23	13	4.7	2.1	1	0.0019			C
87210	K0 III	1.061	0.02	118	16.2	2.2	3	0.0015			
87623	G8 III	0.911	0.92	45	8.8	2.4	3	0.0016			C
88009	G8 III[a]	1.026	0.64	64	11.6		1	0.0020			C
88476	G8 III	0.897	1.00	41	8.4	1.9	3	0.0014			C
88547	K1 III	1.139	−0.40	189	21.8	2.5	1	0.0022			C
88581	K0 III	0.867	0.56	60	9.9	4.3	1	0.0020			C
88748	K3 III	1.289	−1.35	543	41.4	2.6	1	0.0041	6	0.4	
89557	G8 III	0.886	0.17	87	12.1	5.5	3	0.0016			
89993	K0 III	1.062	0.97	49	10.5	2.3	3	0.0014			C
90127	K2 III	1.114	0.39	88	14.6	3.0	1	0.0025			C
90507	G8 III	0.891	1.35	30	7.1	2.6	1	0.0014			C
90990	K1 III	1.078	0.48	79	13.4	2.9	3	0.0017			C
91286	K0 III	0.987	0.88	50	9.9	1.6	3	0.0016			
91318	K2 III	1.028	0.77	57	11.0	1.5	1	0.0022			
91684	G7 III	0.888	0.99	41	8.3	1.9	1	0.0016			
94177	K2 III	1.048	1.56	28	7.8	0.4	1	0.0015			
94425	K0 IV	0.926	1.71	22	6.3	1.8	1	0.0013			C
94669	K2 III[a]	1.100	1.05	48	10.6		3	0.0015			
104130.....	G8 III	0.898	−0.39	148	15.9	0.8	1	0.0014			C
105089.....	K0 III	0.960	0.33	81	12.4	3.2	1	0.0013			
105264.....	G8 III	0.900	0.20	86	12.1	1.5	1	0.0009			
106270.....	G5 IV	0.722	2.79	7	2.9	2.6	1	0.0024	5:	5.1	C
107485.....	G8 III	0.916	0.10	95	12.9	6.6	3	0.0014			
108174.....	K2 III[a]	1.084	1.83	23	7.3		1	0.0017			
108225.....	G9 III[a]	0.938	0.74	54	9.9		2	0.0018			M
108973.....	K0 III	1.010	0.95	48	9.9	1.9	1	0.0015			C

TABLE 1—*Continued*

HD Number (1)	Spectral Type (2)	$(B-V)_0$ (3)	M_V (mag) (4)	L ($L_\odot$) (5)	R ($R_\odot$) (6)	$v \sin i$ (km s^{-1}) (7)	Number of Seasons (8)	σ_{short} (mag) (9)	Timescale (days) (10)	$i_{predict}$ (deg) (11)	*Hipparcos* Variability Type (12)
109551.....	K4 III	1.271	−1.30	507	39.5	2.6	1	0.0044	6:	0.4	
109701.....	G0 IV:	0.681	1.69	19	4.6	9.9	1	0.0075	17	46	M
109822.....	K4 III	1.349	−0.60	297	32.1	3.1	1	0.0032	5:	0.5	
111812.....	G0 III[a]	0.658	−0.01	88	9.7		4	0.0023	7:	54	C
112975.....	M0 III	1.398	−1.45	701	51.1	2.8	1	0.0109	7	0.4	U
112989.....	K1 III	1.098	−2.54	1297	55.3	12.0	4	0.0050	70	17	M
113253.....	K0 III	0.977	0.46	73	11.9	1.4	2	0.0016			
113983.....	G7 III	0.732	0.68	49	7.8	2.4	1	0.0017			
114417.....	K3 III	1.195	0.45	92	15.8	2.6	1	0.0020			C
114946.....	G8 IV	0.853	2.34	11	4.3	3.1	6	0.0016			
117304.....	K0 III	1.032	0.98	47	10.1	1.5	4	0.0013			
119826.....	K2 III	1.159	1.50	33	9.3	2.9	1	0.0026			
120199.....	K3 III	1.254	0.85	68	14.3	2.6	1	0.0045	4	0.8	
120602.....	G5 III	0.869	0.44	67	10.4	1.8	3	0.0018			C
121107.....	G4 III	0.794	−1.07	254	18.9	15.8	4	0.0020			
122548.....	K0 III	1.030	0.89	51	10.4	1.8	1	0.0021			C
122834.....	K2 III	1.141	1.36	37	9.7	1.9	3	0.0019			C
123232.....	M0 III	1.450[c]	−1.96	1242	71.0	4.6	1	0.0125	12	0.9	U
124117.....	K0 III	0.950	0.91	47	9.3	2.2	1	0.0017			C
124572.....	K0 III	1.030	0.44	78	12.8	2.6	1	0.0021			C
125711.....	G8 III	0.896	−1.10	283	22.0	3.0	1	0.0024			C
128200.....	K2 III	1.188	1.19	46	11.2	3.9	1	0.0019			C
128461.....	G8 III	0.814	1.03	37	7.4	3.4	3	0.0017			C
140716.....	K0 III	1.058	1.10	44	9.8	1.9	6	0.0012			C
143209.....	K2 III	1.081	0.78	60	11.7	2.3	3	0.0015			C
144015.....	K2 III	1.240	−0.24	182	23.1	3.2	1	0.0027			
145004.....	K2 III	1.142	1.29	40	10.0	3.7	1	0.0017			C
145894.....	K0 III	1.030	0.55	70	12.2	2.4	3	0.0013			C
145895.....	M0 III	1.547[c]	−2.58	2849	117.7	2.7	1	0.0086	10	0.3	
145957.....	K2 III	1.198	−0.95	334	30.3	2.0	1	0.0027			
150050.....	K2 III	1.246	1.32	44	11.4	2.4	6	0.0021			
154815.....	K1 III	1.078	1.38	34	8.9	2.5	3	0.0015			C
155028.....	G6 II	1.254	−1.56	627	43.3	1.8	1	0.0022			
155038.....	K5 III	1.456	−0.66	380	39.5	2.5	1	0.0061	5	0.4	
155136.....	K2 III	1.097	0.66	68	12.6	1.1	1	0.0019			C
156296.....	K2 III	1.089	0.85	57	11.5	1.6	1	0.0017			
156910.....	K2 III	1.115	0.68	68	12.8	1.3	1	0.0019			
157911.....	K0 III	0.916	0.17	89	12.6	4.0	2	0.0017			
159544.....	K2 III	1.224	0.63	81	15.2	2.6	1	0.0015			
159887.....	K2 III					2.3	1	0.0020			N/A
159966.....	G9 III[a]	1.061	0.90	52	10.8		1	0.0019			C
160385.....	K4 III	1.487	0.02	219	30.7	2.0	4	0.0040			
160507.....	K0 III	0.958	0.66	59	10.6	2.2	3	0.0014			
160823.....	G1 II:	0.840	−0.51	157	15.6	9.1	4	0.0035	25	17	
165195.....	K1: III[d]	1.122	−1.34	441	32.8	2.7	1	0.0074	10	0.9	M
166284.....	K2 III	1.184	0.83	64	13.1	2.5	1	0.0019			
166460.....	K2 III	1.173	−0.11	150	19.9	2.0	1	0.0019			C
166640.....	G8 III[a]	0.883	−0.16	118	14.0		4	0.0013			
166955.....	G8 III	0.905	−1.21	317	23.4	3.3	3	0.0013			C
167587.....	K0 III	0.953	0.66	59	10.5	3.7	1	0.0015			
168619.....	G8 III	0.884	1.61	23	6.2	1.8	3	0.0013			
175589.....	K5 III	1.491	−0.95	538	48.4	2.4	1	0.0068	8	0.4	M
177251.....	G8 III	0.849	0.03	96	12.3	5.4	1	0.0028			
177370.....	K5 III					2.2	1	0.0035	2		N/A
181380.....	K1 III					1.3	1	0.0015			N/A
182567.....	K3 III	1.186	0.47	89	15.5	2.6	1	0.0021			
182896.....	K2 III	1.105	1.72	26	7.8	2.3	1	0.0016			
183387.....	K2 III	1.272	−0.23	189	24.1	1.6	3	0.0016			C
183909.....	K4 III	1.354[c]	−1.46	659	48.0	3.9	1	0.0046	10	0.9	
185018.....	G1 II:	0.796	−2.02	611	29.5	8.4	4	0.0017			
188256.....	G8 III	0.851	−0.27	127	14.2	5.5	1	0.0021			
189533.....	K0 III	1.120	−2.93	1909	68.2	4.5	3	0.0024			
190940.....	K3 III	1.283	−1.07	415	36.0	3.3	4	0.0022			C

TABLE 1—*Continued*

HD Number (1)	Spectral Type (2)	$(B-V)_0$ (3)	M_V (mag) (4)	L ($L_\odot$) (5)	R ($R_\odot$) (6)	$v \sin i$ (km s^{-1}) (7)	Number of Seasons (8)	σ_{short} (mag) (9)	Timescale (days) (10)	$i_{predict}$ (deg) (11)	*Hipparcos* Variability Type (12)
192274.....	K3 III	1.224	0.02	142	20.1	2.5	1	0.0020			C
192800.....	K2 III	1.101	0.52	78	13.6	1.5	1	0.0019			
196229.....	K0 III	1.065	0.85	55	11.1	1.6	1	0.0027			
196642.....	K0 III	0.987	1.11	40	8.9	2.3	1	0.0028			C
196643.....	K5 III	1.496	−1.16	661	53.9	2.4	1	0.0093	7	0.4	
196688.....	K2 III					4.3	1	0.0022			N/A
197274.....	G8 III	0.976	1.38	31	7.8	2.2	2	0.0016			C
197644.....	G7 III	0.907	−0.18	123	14.6	2.2	2	0.0019			C
200413.....	K0 III	0.926	0.00	106	13.8	2.0	2	0.0020			C
200497.....	G8 III	0.857	−0.41	146	15.2	2.8	2	0.0016			D
200577.....	G8 III	0.962	−0.57	185	18.8	2.8	1	0.0022			C
200644.....	K5 III	1.599	−1.16	949	72.1	4.6	1	0.0037	10	0.7	
201053.....	K0 III					3.6	1	0.0020			N/A
201298.....	M0 III	1.607	−1.10	934	72.3	3.4	1	0.0137	12	0.6	M
202573.....	G8 IV	0.843	0.55	60	9.6	2.1	4	0.0017			C
202975.....	G8 III	0.883	−1.45	387	25.4	2.8	4	0.0020			C
203344.....	K0 III	1.036	0.84	54	10.8	2.0	2	0.0014			C
205603.....	G8 III	0.907	0.71	54	9.7	1.5	3	0.0053	240	47	
208530.....	M0 III	1.559	0.58	161	28.3	2.7	1	0.0146	15:	1.6	C
209396.....	G8 III	0.939	0.88	47	9.3	2.2	1	0.0014			C
209408.....	K2 III	1.299	0.35	115	19.2	2.2	1	0.0029			
210269.....	G8 III	0.931	0.83	49	9.4	1.3	3	0.0021			
215427.....	K5 III	1.454[c]	−3.84	7075	170.0	6.3	3	0.0106	30	1.3	U
216143.....	G8: III[d]	0.875	0.03	99	12.7	2.6	2	0.0033			C

[a] Spectral type from literature.
[b] Spectral type estimated from $(B-V)_0$ and *Hipparcos* parallax.
[c] Parallax from *Hipparcos* Catalogue converted to the sum of the parallax and its error for computation of $(B-V)_0$.
[d] Extremely metal-poor. See notes on individual giants in Appendix A.

Sample 2, a group of eight giants, comes from Hall's (1995) list of 17 candidates identified in the GCVS (Kholopov 1985) as K giant pulsating variables. Eight of Hall's 17 giants are not included in our sample because they are either too faint for our APTs or too far south to observe from Arizona. A ninth (AW CVn) was not included since Keenan & McNeil (1989) have classified it as M3 III. The eight giants in sample 2 were observed with a 0.40 m APT and are listed in Table 2 by HD number and variable star name, along with results to be described below.

Sample 3, another group of eight giants observed with the 0.40 m APT, comes from Hatzes & Cochran (1998), who listed 10 K giants, bright giants, and supergiants for which small-amplitude, radial velocity variations have been observed. The periods of these oscillations range from a few to several hundred days. We excluded α Boo from this group because it is too bright for our APTs; in addition, we did not observe the 10th star, γ Cep. We note that α Tau appears in both samples 2 and 3. These eight giants are listed in Table 3 by HD number and Bayer designation, along with results to be described below.

TABLE 2

SAMPLE 2 GIANTS AND ANALYSIS RESULTS

HD Number (1)	Variable Name (2)	Spectral Type[a] (3)	$(B-V)_0$ (4)	Date Range (JD −2,400,000) (5)	N_{obs} (6)	σ_{short} (mag) (7)	Photometrically Variable (8)	GCVS Amplitude (mag) (9)	*Hipparcos* Variability Type (10)
7681	V538 Cas	M0 III[b]	1.604	50,391–50,426	84	0.0098	Yes	1.2	U
29139	α Tau	K5 III	1.533	50,391–50,900	172	0.0069	Yes	0.2	M
36217	CK Ori	K2 III	1.237	50,391–50,547	85	0.0038	No	1.2	C
153210.....	κ Oph	K2 III	1.154	50,466–50,635	120	0.0046	?	0.9	
155526.....	V463 Her	K0 III[c]	0.933	50,474–50,636	123	0.0049	?	0.05	
156947.....	VW Dra	K1.5 III	1.054	50,392–50,642	102	0.0050	?	1.0	
172829.....	HK Aql	K5 III	1.48	50,392–50,642	68	0.0085	Yes	1.0	N/A
198134.....	T Cyg	K3 III	1.264	50,392–50,642	93	0.0061	Yes	0.05	

[a] Spectral type from literature except where noted.
[b] Spectral type, $v \sin i = 3.6$ km s^{-1} and radial velocity $= -29.3$ km s^{-1}, this paper.
[c] Spectral type, $v \sin i = 2.7$ km s^{-1} and radial velocity $= -10.5$ km s^{-1}, this paper.

TABLE 3

SAMPLE 3 GIANTS AND ANALYSIS RESULTS

HD Number (1)	Name (2)	Spectral Type[a] (3)	$(B-V)_0$ (4)	Date Range (JD −2,400,000) (5)	N_{obs} (6)	σ_{short} (mag) (7)	Photometrically Variable (8)	Radial Velocity Periods (days) (9)	*Hipparcos* Variability Type (10)
29139.....	α Tau	K5 III	1.533	50,391–50,900	172	0.0069	Yes	1.8, 50, 643	M
62509.....	β Gem	K0 III	0.988	50,718–50,949	108	0.0038	No	558	M
156283.....	π Her	K3 II	1.410	50,721–50,997	97	0.0054	Yes[b]	90, 613	M
161096.....	β Oph	K2 III	1.162	50,725–50,997	93	0.0053	?	0.237, 0.255, 13	
164058.....	γ Dra	K5 III	1.510	49,747–50,997	481	0.0061	Yes	3.5, 5.7, 333	M
183912.....	β^1 Cyg	K3 II	1.059	50,718–50,997	95	0.0055	?	7.5, 213	D
187076.....	δ Sge	M2 II+B:	1.280	50,713–50,996	113	0.0438	Yes[c]	2.0	U
206778.....	ε Peg	K2 Ib–II	1.559	50,718–50,996	97	0.0109	Yes	46, 65, 538	U

[a] All spectral types from literature.
[b] Period of 95 ± 4 days seen in *B* but not in *V* data.
[c] Possible periods of 33 and 72 days.

3. OBSERVATIONS

3.1. *Spectroscopic Observations*

High-dispersion spectroscopic observations were obtained with the KPNO coudé feed telescope, coudé spectrograph, and a Texas Instruments CCD. The red wavelength spectra centered at 6430 Å have a resolution of 0.21 Å, a wavelength range of about 80 Å, and a typical signal-to-noise ratio of 200. Additional blue wavelength spectra were centered at 3950 Å to include the Ca II H and K lines. Those spectra have a wavelength range of 56 Å and a resolution of 0.21 Å.

Bias subtraction, flat-field division, wavelength calibration, and continuum rectification were performed on the raw spectra with the programs in IRAF. Thorium-argon comparison spectra were obtained at intervals of 1–2 hr. The wavelength solution for a program star spectrum was applied by interpolating in time between the two comparison spectra that bracketed the stellar observation.

At least one red wavelength spectrogram was obtained for 147 of our 187 giants with the spectroscopic sample biased toward the fainter giants of the photometric sample, most of which have only HD spectral types and typically few, if any, references in the SIMBAD database. Our red wavelength spectra were used to determine spectral types, measure radial velocities, and compute projected rotational velocities of the giants. For about 33% of the spectroscopic subsample, blue wavelength spectra were obtained to measure Ca II H and K surface fluxes.

3.2. *Photometric Observations*

The photometric observations in this survey have been obtained between 1993 April and 1998 July with three automatic photoelectric telescopes (APTs) at Fairborn Observatory. Until 1996 July, Fairborn was located at the Fred L. Whipple Observatory on Mount Hopkins. During the summer of 1996, the APTs were relocated to Fairborn Observatory's new site at Washington Camp (altitude 5700 feet) in the Patagonia Mountains of southern Arizona (Eaton, Boyd, & Henry 1996).

The 0.4 m (T3) APT observes in the Johnson *B* and *V* bandpasses. Details on the telescope and photometer, observing sequences, and reduction of the data can be found in Henry (1995a, 1995b) and Henry et al. (1995b). External precision of the group means, defined as the standard deviation of a single nightly group mean from the seasonal mean, is about 0.004 mag on good nights for pairs of constant stars. This is roughly the scintillation noise expected in these observations.

The 0.75 m (T4) and 0.80 m (T8) APTs both observe in Strömgren *b* and *y* bandpasses. Details on the equipment, observing sequences, and data reduction can be found in Henry (1999). The *b* and *y* observations are combined into a single value, $(b + y)/2$, to increase precision, as done by Lockwood, Skiff, & Radick (1997) in their program of manual photometry of solar-type stars. External precision of the 0.75 m APT observations averages about 0.0014 mag on good nights; precision of the 0.80 m APT is about 0.0011 mag. Like the 0.4 m APT, scintillation noise is the dominant source of error for these APTs.

All three telescopes make extensive observations of standard stars each night to determine the nightly extinction as well as to track any long-term instrumental changes. Since the APTs collect data whenever they can find stars, they sometimes do so under nonphotometric conditions. We therefore use the standard deviation of the group mean magnitudes (a measure of the internal precision) as well as the results of the standard star observations to reject data taken during poor or marginal conditions. Specifically, group means from the 0.4 m APT with standard deviations larger than 0.01 mag are discarded; group means from the 0.75 and 0.80 m APTs with standard deviations larger than 0.005 mag are discarded. Further, only 0.75 and 0.80 m APT observations made on nights when the all-sky reduction of the standard stars gave good results are used in the analysis.

4. ANALYSES

Tables 1–5 present the results of our photometric and spectroscopic analyses.

Table 1 summarizes the spectroscopic and photometric properties derived for the giants in sample 1. Column (1) identifies each giant by its HD number. Column (2) lists our spectral type, if determined, or the best spectral type from the literature. Column (3) gives the $(B-V)_0$ value. Columns (4), (5), and (6) give our computed values of absolute magnitude M_V, luminosity *L*, and radius *R*. Column (7) lists our $v \sin i$ value. Columns (8) and (9) give the number of photometric observing seasons and the standard deviation of the

nightly brightness measurements, $\sigma_{\rm short}$, respectively. Column (10) gives the timescale of photometric variation if it can be estimated from the light curve. Column (11) gives $i_{\rm predict}$, the predicted inclination of a star's rotation axis assuming the observed photometric variability is due to rotational modulation. Finally, column (12) lists the type of photometric variability from the *Hipparcos* Catalogue. These results are described in more detail in the following paragraphs.

Our spectral types in column (2) of Table 1 were determined by visual comparison with stars from the list of Keenan & McNeil (1989). Spectra of those reference stars were obtained with the same KPNO coudé feed setup used for most of the program star observations. Strassmeier & Fekel (1990) identified several luminosity sensitive and temperature sensitive line ratios in the 6430–6465 Å region. Those critical line ratios and the general appearance of the spectrum were employed as spectral-type criteria. The line ratios used to determine the luminosity class lose much of their sensitivity in early-G giants, making most of those classifications more uncertain. Classification was also more difficult for several very metal-poor giants, for which no grid of similar standards was available. Greater uncertainty in such classifications is indicated by a colon. If no red wavelength spectrum was obtained for a star, the literature was searched for its best spectral type. When available, the spectral types of Keenan & McNeil (1989) were preferred. Only as a last resort have unreferenced spectral types from The Bright Star Catalogue (Hoffleit & Jaschek 1982) been used.

The values of $(B-V)_0$ listed in column (3) of Table 1 were computed in the following manner. The *Hipparcos* parallaxes (Perryman et al. 1997) indicate that most of our giants have distances between 100 and 300 pc, implying observed colors that are moderately affected by interstellar extinction. Thus, unreddened colors computed with various mean extinction values were compared with unreddened colors (Johnson 1966; FitzGerald 1970) assumed from our spectral classifications. From that comparison, $A_v = 0.8$ mag kpc^{-1} has been adopted, with $E(B-V) = A_v/3.3$, and the $(B-V)_0$ colors of Table 1 have been computed accordingly. In four cases where the *Hipparcos* parallax was comparable to or smaller than its error (or even negative), the parallax was replaced with the sum of the parallax and its error for computations of $(B-V)_0$.

Column (4) lists the M_v determined from our adopted reddening law and the *Hipparcos* parallax except in the four cases, noted in column (3), where the *Hipparcos* parallax was replaced by the sum of the parallax and its error. The resulting luminosity and radius are given in columns (5) and (6), respectively. The luminosity was determined from M_v, the bolometric correction of Flower (1996), and an assumed $M_{\rm bol} = 4.75$ mag for the Sun. The radius was then computed by assuming the $(B-V)_0$ versus $T_{\rm eff}$ relationship of Flower (1996).

Our measured $v \sin i$ values given in column (7) of Table 1 were determined from the red wavelength spectra with the procedure of Fekel (1997). Most of the projected rotational velocities have uncertainties of 0.5–1.0 km s^{-1}. The uncertainties may be greater for those giants having the lowest rotational velocities since the line widths of those giants are dominated by macroturbulence rather than rotation. In addition, increased uncertainty is also likely for the coolest giants whose spectra have the severest line blending. If more than one red wavelength spectrum was obtained for a giant, the given value is an average.

The short-term standard deviations, $\sigma_{\rm short}$, in column (9) of Table 1 are means of the seasonal values computed from the number of observing seasons given in column (8). Within a single observing season, the quantity $\sigma_{\rm short}$ is defined as the standard deviation of a single, nightly mean differential magnitude from the corresponding seasonal mean differential magnitude and thus represents the level of short-term or night-to-night photometric variability in each of the giants. The giants in Table 1 were all observed with the 0.75 or 0.80 m APTs. Since these two telescopes made their observations with identical procedures and have nearly identical external precisions ($\sim$0.0012 mag), the standard deviations from the two telescopes can be directly compared.

The computation of these seasonal values of $\sigma_{\rm short}$ requires some additional explanation. Our giants were all observed as members of groups consisting of three comparison stars and one program star, with each giant serving as one of the comparison stars of its group. Therefore, differential magnitudes of each giant were computed against each of the other three stars in the group. If each of those three stars (including our original program star) was constant, as determined by the intercomparison of the standard deviations of the various pairs, then $\sigma_{\rm short}$ represents the average of the short-term standard deviations determined against each of those three stars. If only two of the other stars proved to be constant, then $\sigma_{\rm short}$ is the mean determined with the two constant stars as comparisons.

When two of the three potential comparison stars for a G or K giant were eliminated because they were both variable, then the interpretation of any variability in the remaining pair of stars can become ambiguous. If $\sigma_{\rm short}$ for this remaining pair was small (i.e., at or near the external precision limit of 0.0012 mag for these telescopes), then obviously both stars are constant and the giant was retained in our study. If $\sigma_{\rm short}$ for this remaining pair was large compared to the limit of precision, then one or both of the stars are variable. Sometimes, the comparison star for the giant in this remaining pair was one of our solar-type program stars. If that solar-type star is roughly solar age or older, then its photometric variability will be very small (see next paragraph). If variability can be detected in those cases, then the variability can be attributed confidently to the giant star and not to its only remaining comparison star, and the giant was retained in the study. In the few cases where we could not judge whether the giant or its only remaining comparison was the variable, the giant was removed from our study and does not appear in Table 1. Therefore, since multiple comparison stars were observed in each group, we can be sure that all comparison stars used to derive $\sigma_{\rm short}$ for the giants in Table 1 are constant to the limit of our precision.

To determine what value of $\sigma_{\rm short}$ can be adopted to establish unambiguous variability in our giants, we take advantage of the decreasing trend in photometric variability with age in Sun-like stars shown in Figure 11 of Henry (1999). There, short-term variability in a sample of 150 Sun-like stars is plotted against $\log R'_{\rm HK}$, a measure of the surface magnetic activity in these stars. For the 72 stars with $\log R'_{\rm HK} < -4.90$ (i.e., the stars roughly solar age or older that should have very low photometric variability), over 80% of the values of $\sigma_{\rm short}$ are less than 0.0015 mag, and *all* are less than 0.0020 mag. This demonstrates experimentally

that pairs of constant stars will have values of σ_{short} less than 0.0020 mag when measured and processed with the procedures of Henry (1999). Since all of the observations in sample 1 of this paper were acquired and processed with these identical procedures and equipment, we can conclude that the giants in Table 1 with $\sigma_{short} \geq 0.0020$ are unambiguously variable.

By this criterion, we have detected 73 of the 172 giants in Table 1 (42.4%) as short-term variables. Although many of these variables exhibited coherent variability at least during a portion of the observation interval, periodogram analysis nonetheless failed, in general, to reveal convincing periodicities. Therefore, column (10) of Table 1 gives the timescale of light variations estimated from the light curves of the 30 giants for which this was possible. These timescales represent typical intervals between successive maxima or minima in the light curves. The quantity $i_{predict}$ in column (11) was determined by estimating the rotational velocity of the giant from its radius (col. [6]) and the timescale for light variations. This rotational velocity was ratioed with the observed $v \sin i$ to compute the predicted rotational inclination under the assumption that the light variation is due to rotational effects. The variability type from the *Hipparcos* Catalogue (col. [12]) is given as C (constant), P (periodic variable), M (possible microvariable with an amplitude below 0.03 mag), U (unsolved or nonperiodic variable), D (duplicity-induced variable and not necessarily a true variable), or N/A (star is not listed in the *Hipparcos* Catalogue). A blank in this column indicates that the star could not be classified as variable or constant with any degree of certainty due to one or more outliers in the photometry. Of the 165 stars in Table 1 that are in the *Hipparcos* Catalogue, only 11 (6.7%) are flagged as variable in the Catalogue, versus 42.4% found to be variable from our APT photometry. Comparing the APT photometry with the *Hipparcos* photometry, we find that if the σ_{short} obtained with our APTs is less than about 0.007 mag, corresponding to an amplitude of about 3%, the star is unlikely to be listed as variable in the *Hipparcos* Catalogue.

Table 2 presents our analysis results for the giants in sample 2 observed with the 0.40 m APT. Column (1) lists each giant's HD number and column (2) its variable star designation. Column (3) gives the spectral type from the literature, if available, or in the case of two giants, our classification. Column (4) lists the $(B-V)_0$, computed with our adopted mean interstellar reddening equation. Columns (5) and (6) list the Julian date range and number of photometric observations, respectively. The short-term standard deviation, σ_{short}, is given in column (7). Since these giants were observed with the 0.40 m APT at the somewhat lower precision of 0.004 mag, these values of σ_{short} cannot be compared directly with the results of the sample 1 giants in Table 1. In column (8) we conclude whether the giants are photometrically variable or not, based on the light curves (see § 5), the values of σ_{short}, and our periodogram analyses. For comparison with columns (7) and (8), column (9) gives the amplitude listed in the GCVS (Kholopov 1985), and column (10) gives the *Hipparcos* variability type.

Table 3 presents the analysis results for the giants in sample 3 observed with the 0.40 m APT. Its columns of data are identical to those of Table 2 except for columns (2) and (9). Column (2) gives the Bayer designation, while column (9) gives the radial velocity periods from Hatzes & Cochran (1998).

Table 4 presents the determination of Ca II H and K chromospheric emission fluxes for 48 of the giants in sample 1. The giants for this subsample were selected to span the range of σ_{short} values at various $(B-V)_0$. Column (1) lists the HD number of each star; column (2) gives $(V-R)_0$, determined from our computed $(B-V)_0$ and Table 1 of Johnson (1966). For giants with $(B-V)_0 \leq 0.92$, the $(V-R)_0$ values were extrapolated from the values in Table 1 of Johnson (1966). Columns (3) and (4) list the

TABLE 4

SURFACE FLUXES IN THE Ca II H AND K LINES FOR SELECTED GIANTS IN SAMPLE 1

HD Number (1)	$(V-R)_0$ (mag) (2)	log F(K)[a] (3)	log F(H)[a] (4)	log R'_{HK} (5)
53078.....	0.640	6.09	5.98	−4.31
66285.....	0.520	6.12	5.91	−4.64
70136.....	0.990	4.80	4.69	−5.23
73799.....	0.980	4.89	4.79	−5.14
74485.....	0.670	5.90	5.70	−4.51
84453.....	0.690	5.34	5.29	−5.08
88748.....	0.950	4.97	4.84	−5.09
89993.....	0.780	5.17	5.08	−5.06
94177.....	0.780	5.18	5.10	−5.07
104130	0.680	5.46	5.35	−5.03
105089	0.710	5.27	5.28	−5.06
106270	0.550	5.92	5.87	−4.75
109551	0.930	5.05	4.99	−4.99
109701	0.520	6.44	6.30	−4.16
109822	1.010	4.86	4.73	−5.16
111812	0.510	6.54	6.36	−4.09
112975	1.050	4.97	4.75	−5.06
112989	0.810	5.60	5.49	−4.59
113983	0.560	5.91	5.76	−4.82
120199	0.920	4.94	4.89	−5.11
120602	0.670	5.57	5.50	−4.91
121107	0.600	6.10	6.01	−4.37
122834	0.830	4.98	4.90	−5.17
123232	1.100	4.89	4.72	−5.08
143209	0.800	5.04	4.94	−5.18
145004	0.830	5.02	5.02	−5.09
145895	1.230	4.43	4.27	−5.46
145957	0.870	5.13	5.00	−4.99
150050	0.920	4.68	4.67	−5.36
155038	1.110	4.67	4.59	−5.26
159544	0.890	4.89	4.73	−5.23
160385	1.150	4.41	4.27	−5.52
160823	0.630	6.30	6.16	−4.11
165195	0.820	5.02	5.03	−5.10
175589	1.150	4.67	4.58	−5.23
177251	0.640	5.90	5.68	−4.60
177370	1.200	4.30	4.16	−5.59
183387	0.930	4.79	4.76	−5.24
183909	1.010	4.88	4.81	−5.11
185018	0.600	6.33	6.21	−4.13
190940	0.940	4.95	4.87	−5.09
192274	0.890	5.02	4.90	−5.09
196229	0.790	5.13	5.03	−5.10
196642	0.740	5.30	5.14	−5.06
196643	1.150	4.65	4.53	−5.26
200644	1.480	3.72	3.55	−6.11
201298	1.480	3.71	3.59	−6.10
205603	0.690	5.49	5.43	−4.93

[a] Fluxes in units of ergs cm^{-2} s^{-1}.

TABLE 5

RESULTS OF PHOTOMETRIC ANALYSES OF SELECTED GIANTS FROM SAMPLE 1 THAT WERE REOBSERVED WITH THE 0.40 m APT

HD Number (1)	Date Range (JD −2,400,000) (2)	N_{obs} (3)	σ_{short} (mag) (4)	Photometrically Variable (5)	Timescale (days) (6)	$i_{predict}$ (deg) (7)	*Hipparcos* Variability Type (8)
70136.....	50,729–50,936	126	0.0053	?			
84345.....	50,726–50,984	182	0.0176	Yes	15	0.7	U
88748.....	50,732–50,982	138	0.0101	Yes	10	0.4	
109551	50,770–50,997	136	0.0059	Yes			
109822	50,774–50,997	140	0.0051	Yes			
112975	50,782–50,994	41	0.0121	Yes	10	0.6	U
120199	50,788–50,995	119	0.0046	?			
123232	50,783–50,995	107	0.0185	Yes[a]	20	1.5	U
145895	50,831–50,996	84	0.0087	Yes	10	0.3	
145957	50,718–50,997	139	0.0045	?			
155038	50,711–50,997	140	0.0082	Yes[b]	5	0.4	
165195	50,718–50,997	108	0.0095	Yes	10	0.9	M
175589	50,714–50,996	114	0.0087	Yes			M
177370	50,711–50,996	104	0.0082	Yes			N/A
183909	50,718–50,997	108	0.0056	Yes	25	2.3	
196229	50,724–50,995	92	0.0044	?			
196643	50,721–50,996	97	0.0090	Yes[c]	6	0.3	
200644	50,734–50,995	52	0.0058	?			
201298	50,711–50,996	83	0.0092	Yes	15	0.8	M
208530	50,721–50,996	76	0.0106	Yes	20	2.2	C

[a] Possible periods of 20 and 36 days.
[b] Weak periodicity at 4.82 ± 0.01 days.
[c] Weak periodicity at 5.96 ± 0.02 days.

logarithm of the Ca K and H emission-line fluxes, respectively. Those surface fluxes were determined with the procedures outlined by Linsky et al. (1979) as discussed by Strassmeier et al. (1990). To correct for the photospheric flux, we used the relation of Noyes et al. (1984). Such a correction becomes relatively unimportant for $V-R > 0.74$. Following Strassmeier et al. (1990, 1994a), who obtained Ca II H and K observations with the same telescope and spectrograph setup and determined fluxes in a similar manner, we estimate flux uncertainties of ±25%. Column (5) gives the logarithm of R'_{HK}. This is the chromospheric radiative loss in the H and K lines normalized to the total surface luminosity of the star. The latter was computed with effective temperatures from Flower (1996).

Table 5 presents the results of our photometric analysis of selected giants from sample 1 that were reobserved for a single season with the 0.40 m APT. These giants were chosen from sample 1 for further observation if their photometric amplitudes were $\gtrsim$0.01 mag. Column (1) lists each giant's HD number. Columns (2) and (3) give the Julian date range and number of observations, respectively. The short-term standard deviation, σ_{short}, is listed in column (4); again, this is not directly comparable to those given in Table 1. In column (5) we conclude whether the giants are photometrically variable or not, based on the light curves, σ_{short}, and our periodogram analyses. As before, we did not find convincing evidence for periodicity in any of these giants (but see the footnotes to the table), so column (6) gives our estimated timescale of variation for most of the variables. Column (7) gives $i_{predict}$ values, computed in the same manner as those listed in Table 1, and column (8) lists the *Hipparcos* variability type, described above for Table 1.

5. DISCUSSION

The two leading mechanisms for photometric variability in late-type giants are pulsation and rotational modulation of starspots (e.g., Jorissen et al. 1997). These two mechanisms have also been considered as the cause of radial velocity variations observed in K giants (e.g., Hatzes & Cochran 1993, 1998). Pulsation is recognized as the cause of variability in M giants (e.g., Gautschy & Saio 1996), while starspot modulation is the cause of variability in rapidly rotating single and binary G–K giants (e.g., Strassmeier & Hall 1988a; Strassmeier et al. 1989).

Our spectroscopic observations of 147 of the 187 giants in this study reveal no double-lined spectroscopic binaries. For 66 of the giants we have multiple spectroscopic observations. Although a few of the giants have small velocity variations (see Appendix B), none of them appear to be close binaries. Therefore, our sample of 187 giants is likely to contain few, if any, interacting binaries or secondary components that would significantly affect our derived properties of the giants, and we proceed on the assumption that all of these giants are single or effectively single. Using our observations of the 187 giants in our three samples, we examine whether the variability seen in those giants is characterized better by pulsation or rotation.

Figure 1 plots σ_{short}, which characterizes light variations on night-to-night timescales, versus $(B-V)_0$ for the 165 giants of sample 1 that have *Hipparcos* parallaxes. As explained in § 4 above, stars are identified as variable if $\sigma_{short} \geq 0.0020$ mag. Light variability occurs throughout the range of $(B-V)_0$, corresponding to spectral classes ranging from G0 to M0. Jorissen et al. (1997) found that, for spectral types earlier than about K3 III, the giants in their sample

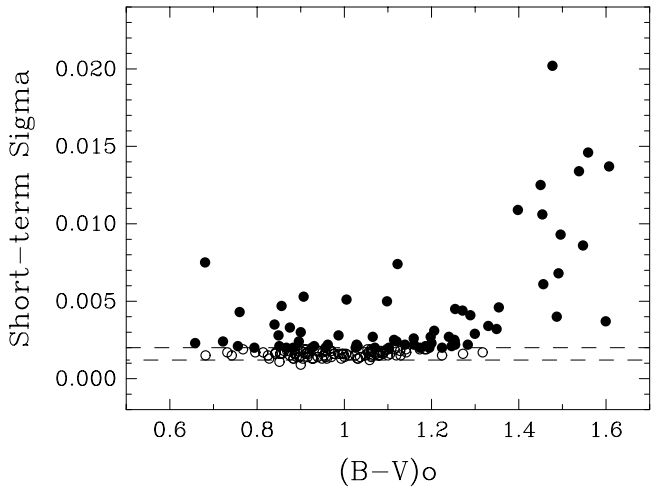

FIG. 1.—Night-to-night light variations, $\sigma_{\rm short}$, plotted against $(B-V)_0$ for the 165 giants of sample 1 that have *Hipparcos* parallaxes. Giants with $\sigma_{\rm short} \geq 0.0020$ mag are variable and are plotted as filled circles; constant giants are plotted as open circles. The lower dashed line represents the limit of precision ($\sim$0.0012 mag) for the 0.75 and 0.80 m APTs. The upper dashed line at 0.0020 mag represents the level at which photometric variability can be detected unambiguously in the observations.

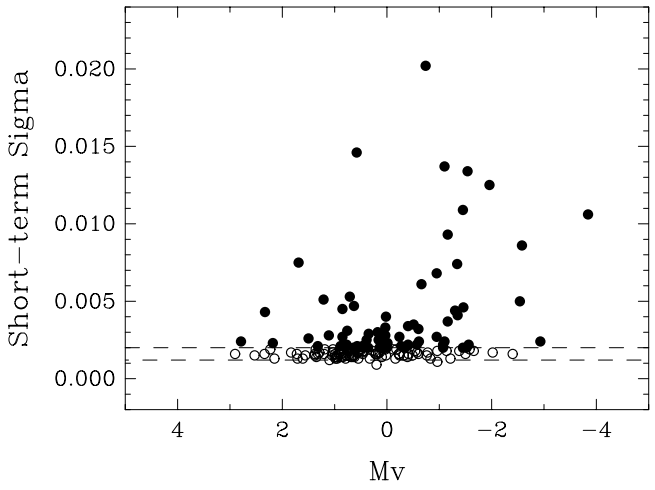

FIG. 2.—Night-to-night light variations, $\sigma_{\rm short}$, plotted vs. absolute visual magnitude, M_v, for the 165 giants of sample 1 that have *Hipparcos* parallaxes. The symbols and dashed lines are as defined for Fig. 1.

were constant to $\sigma \leq 0.006$ mag. They also showed that large-amplitude variability, $\sigma \geq 0.010$ mag, begins for M giants. While we are able to detect lower levels of variability, our results are in general agreement with theirs. For giants with $(B-V)_0 < 1.35$ ($\sim$K3 III or earlier), we find only two with $\sigma_{\rm short} > 0.006$ mag, although many of our giants in this range show variability at levels of 0.002–0.005 mag. In fact, most of the giants with $1.10 \leq (B-V)_0 \leq 1.35$ ($\sim$K1 III–$\sim$K3 III) are variable at such lower levels. The giants with $(B-V)_0 \geq 1.40$ mag ($\sim$K4 III–$\sim$M0 III) are all variable, half with $\sigma_{\rm short} \geq 0.01$ mag.

Table 6 summarizes our detection of photometric variability in these 165 giants as a function of $(B-V)_0$. The percentage of variables is lowest for G6–K1 giants. The fraction of variables increases toward both later and earlier spectral classes. These results are in accord with those of Eyer et al. (1994), who made an initial examination of light variability in the stellar sample observed by *Hipparcos*. They concluded that "G8 III giants appear to be among the most stable stars."

In Figure 2, $\sigma_{\rm short}$ is plotted versus absolute visual magnitude, M_v, for the same group of 165 giants. Variability occurs at all luminosities, although the brightest giants

TABLE 6

PERCENTAGE OF THE 165 SAMPLE 1 GIANTS IN FIGURE 1 THAT EXHIBIT SHORT-TERM VARIABILITY ($\sigma_{\rm short} \geq 0.0020$ mag)

$(B-V)_0$ Range (mag)	Giant Spectral Class	$N_{\rm stars}$	Percentage Variable
0.65–<0.8.....	G0–G2	11	54
0.8–<0.9	G3–G5	28	29
0.9–<1.0	G6–G9	37	19
1.0–<1.1	K0, K1	34	24
1.1–<1.2	K2	23	48
1.2–<1.3	K3	15	87
1.3–<1.4	K4	5	80
1.4–<1.5	K5	7	100
1.5–1.6.....	M0	5	100

($M_v < -0.5$) have a greater percentage of large $\sigma_{\rm short}$ values. Constant giants, however, appear at essentially all luminosities.

Figure 3 is a three-dimensional H-R diagram, plotting photometric variability versus M_v and $(B-V)_0$ for the same group of 165 giants. As in the previous two figures, constant giants are identified with open circles, but here variable giants are plotted as filled circles with sizes that scale with $\sigma_{\rm short}$. This figure maps the distribution of variability in both luminosity and temperature and so combines the results of Figures 1 and 2. The approximate location of the coronal dividing line (CDL) from Haisch (1999) is given in the figure. The CDL separates giants with hot coronae on the left from giants with cool, massive winds on the right. As noted above, photometric variability occurs at all values of $(B-V)_0$, but we see here that the largest amplitudes occur to the right of the CDL. The segregation of our sample by the CDL, along with the larger observed amplitudes on the right, suggests that different variability mechanisms might be operating on opposite sides of the CDL. Several individual giants to the left of the CDL are labeled and discussed further below.

In some late-type stars, the interplay of convection and rapid rotation results in a magnetic dynamo that produces chromospheric activity and starspot variability. However, rapid rotation is not a typical property of single late-type giants. De Medeiros, da Rocha, & Mayor (1996) have used a survey of rotational velocities for about 1100 single F5–K5 giants to determine the mean projected rotational velocity as a function of spectral type. For early G giants the mean projected rotational velocity is 6.4 km s^{-1}. This decreases to 3.3 km s^{-1} for mid-G giants and then to about 2.0 km s^{-1} for late G and K giants. Rapidly rotating, late-type giants are rare and usually the result of tidal forces in a close binary (e.g., Henry et al. 1995a). However, more than 15 *single* late G and early K giants having $v \sin i$ of 6–50 km s^{-1} have been found via their very significant chromospheric activity (Fekel & Balachandran 1993, 1994). Such single giants, like their binary counterparts, show light variations that are the result of starspot modulation.

Figure 4 compares $\sigma_{\rm short}$, indicated by the size of the plotted symbols, to $(B-V)_0$ on the x-axis and $v \sin i$ on the

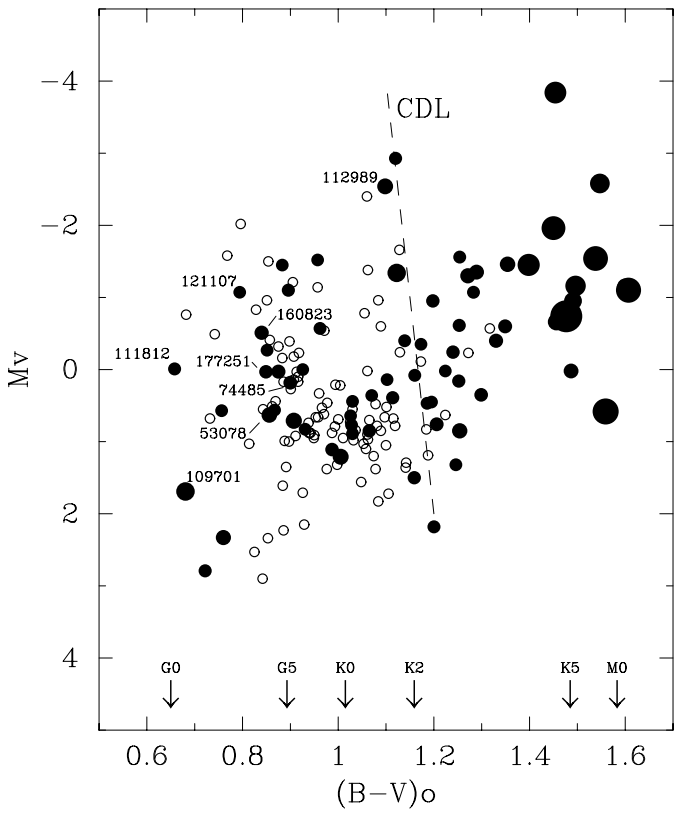

FIG. 3.—Three-dimensional H-R diagram, plotting variability vs. M_v and $(B-V)_0$ for the same giants as in Figs. 1 and 2. While constant giants are identified with open circles, as in the previous two figures, variable giants are plotted as filled circles with sizes that scale with σ_{short}. The coronal dividing line (CDL), separating giants with hot coronae on the left from those with cool, massive winds on the right, is shown. Eight of the giants to the left of the CDL are labeled with their HD numbers and are discussed in the text. Arrows indicate colors for selected giant spectral classes.

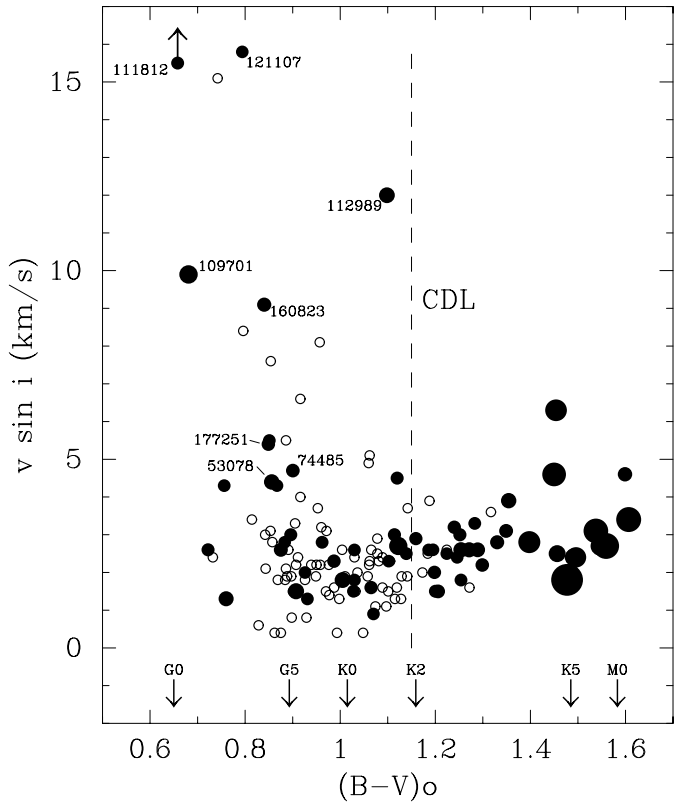

FIG. 4.—Three-dimensional plot comparing σ_{short} to $(B-V)_0$ on the x-axis and v sin i on the y-axis for the 139 giants in sample 1 that have $(B-V)_0$ and our measured values of v sin i. Symbols and identifications are the same as in Fig. 3. The v sin i for HD 111812 falls outside the plotted range.

y-axis for the 138 giants in sample 1 that have $(B-V)_0$ and our measured values of v sin i. The vast majority of these giants have v sin i values between 1 and 3 km s^{-1}, but the tail of the distribution extends to about 15 km s^{-1}. This velocity distribution is similar to that of the single giants in De Medeiros et al. (1996). We added HD 111812 (31 Comae) from sample 1 to the figure, based on its published v sin i value of 57 km s^{-1} (Strassmeier, Washüttl, & Rice 1994b) but note that its v sin i lies outside the range plotted. We have also plotted the approximate location of the CDL from Haisch (1999). The figure divides into four regions, based on the observed variability patterns. The upper right region of the figure [$(B-V)_0$ to the right of the CDL and v sin $i \geq 9$ km s^{-1}] is vacant since single K and M giants generally have low v sin i values (De Medeiros et al. 1996). The giants in the lower right region [$(B-V)_0$ to the right of the CDL but with low v sin i] are nearly all variable and have the highest variability amplitudes. The majority of giants in the lower left region [$(B-V)_0$ to the left of the CDL and low v sin i] are constant, but a significant fraction (30%) do show low-amplitude variability. Finally, the upper left region [$(B-V)_0$ to the left of the CDL and v sin $i \geq 9$km s^{-1}] contains only a few giants, and most are variable. The same eight giants labeled in Figure 3 have also been identified in this figure.

Figure 5 plots $\sigma_{\rm short}$ with symbols as in Figure 4 but against $(B-V)_0$ on the x-axis and our measured values of log $R'_{\rm HK}$ on the y-axis for 47 giants from sample 1. The vertical dashed line is the CDL. The horizontal dashed line at log $R'_{\rm HK} = -4.7$ corresponds to the lower limit of enhanced chromospheric activity used as a criterion for inclusion in the Catalog of Chromospherically Active Binary Stars (Second Edition) (Strassmeier et al. 1993). We note, however, that most stars considered to be chromospherically active have log $R'_{\rm HK} > -4.0$ (Fig. 5*b* of Strassmeier et al. 1990) and so would lie above the upper limit of our plot. Eight of the 10 giants with log $R'_{\rm HK} > -4.7$ are variable, and all lie to the left of the CDL. These eight chromospherically active variables are labeled in the figure and are the same eight giants labeled in Figures 3 and 4.

The variable giants with the largest photometric amplitudes lie in the lower right region of Figure 5, to the right of the CDL and below the lower limit for enhanced chromospheric activity. These giants are probably too weak magnetically to produce significant photometric variations via rotational modulation of surface features. Therefore, we suggest that the variability mechanism operating in M giants—pulsation—is also operating in the giants in the lower right region of Figure 5.

In the upper left region of Figure 5, to the left of the CDL and above the lower limit for enhanced chromospheric activity, there are 10 giants. As noted above, eight of these 10 chromospherically active giants are photometrically variable; five of these eight variables also have v sin $i \geq 9$ km s^{-1} and so lie in the upper left region of Figure 4. This combination of chromospheric activity and rapid rotation suggests that the variability mechanism in these five giants may be due to rotational modulation of active regions.

The combination of our photometric and spectroscopic observations, along with the *Hipparcos* results, allows us to

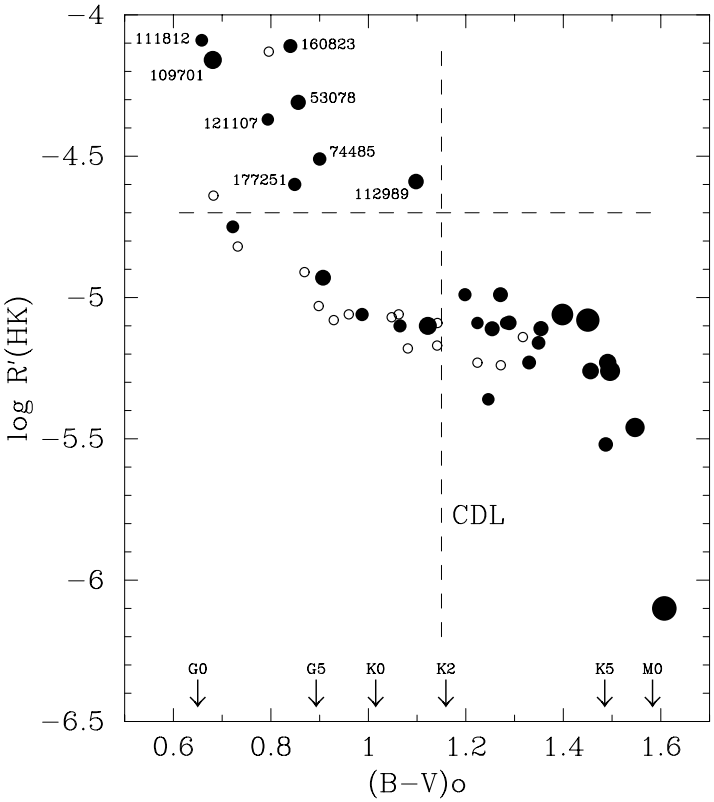

FIG. 5.—Three-dimensional plot comparing $\sigma_{\rm short}$ to $(B-V)_0$ on the x-axis and log $R'_{\rm HK}$ on the y-axis for the 47 giants from sample 1 that have $(B-V)_0$ and our measured values of log $R'_{\rm HK}$. Symbols and identifications are the same as in Fig. 3. The horizontal dashed line corresponds to the lower limit of enhanced chromospheric activity from Strassmeier et al. (1993). The eight variable giants that lie to the left of the CDL and above the limit for enhanced chromospheric activity are labeled in this figure and are the same eight giants labeled in Figs. 3 and 4.

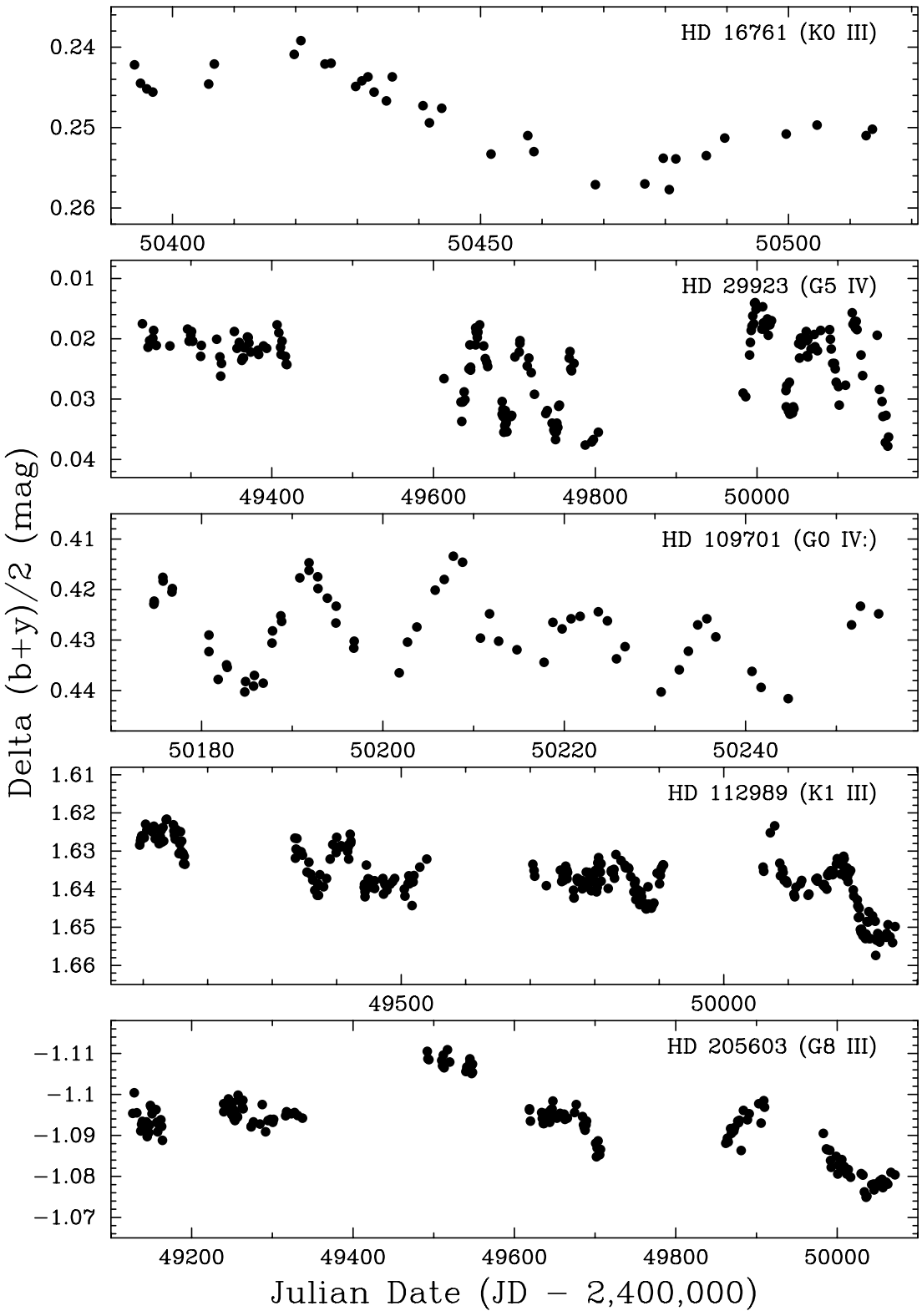

FIG. 6.—Selected light curves of giants from sample 1 observed with the 0.75 or 0.80 m APT. These light curves were used to determine the timescales of photometric variability given in Table 1. Note that the *x*- and *y*-scales vary from panel to panel.

test the rotational modulation hypothesis. Photometric light curves of selected giants with amplitudes sufficient to determine timescales of variability are shown in Figures 6 and 7. Figure 6 plots light curves of five giants from Table 1 observed with the 0.75 or 0.80 m APT. Figure 7 plots light curves of four of the sample 1 giants that were reobserved with the 0.40 m APT (Table 5) plus one giant from sample 3 (Table 3), also observed with the 0.40 m APT. For 29 giants from sample 1, we used the photometric timescales, the radii computed from the *Hipparcos* parallaxes and our $(B-V)_0$ colors, along with our observed $v \sin i$ values to derive the quantity $i_{\rm predict}$, which gives the inclination of a star's rota-

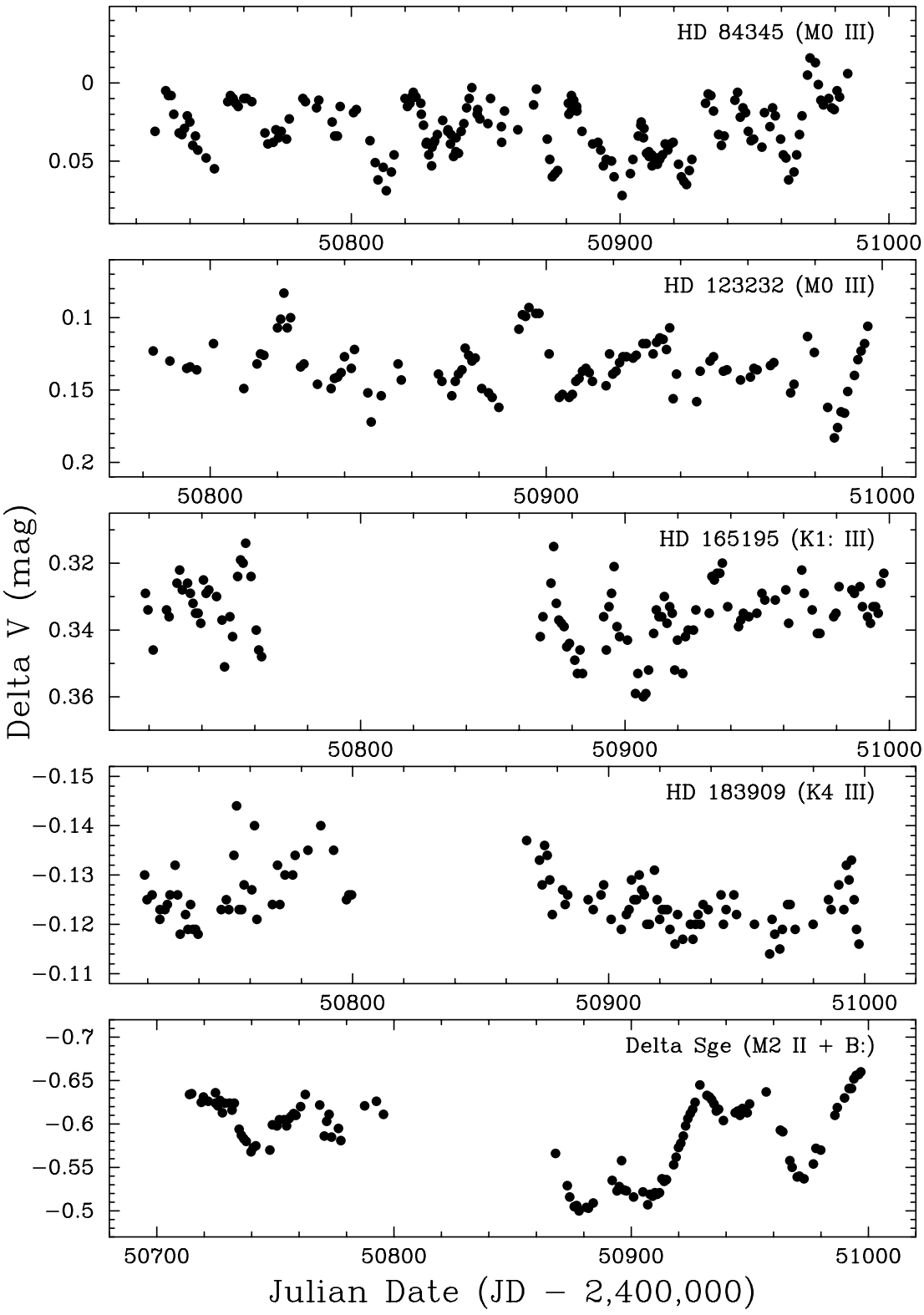

FIG. 7.—Selected light curves of giants from sample 1 (*top four panels*) reobserved with the 0.40 m APT. These light curves were used to determine the timescales of photometric variability given in Table 5. The bottom panel includes one of the giants from sample 3. Note that *x*- and *y*-scales vary from panel to panel.

tion axis *assuming* the photometric variability is due to rotational modulation. All of the predicted rotational inclinations from Tables 1 and 5 are plotted as filled circles against $(B-V)_0$ in Figure 8. If a giant has $i_{\rm predict}$ values determined from both of the independent data sets in these two tables, the mean value is plotted in the figure. The approximate location of the CDL is also indicated. Since our sample of randomly selected field giants must have randomly oriented axes of rotation, half of the giants should have inclinations greater than 60° (Russell, Dugan, & Stewart 1938). Instead, we find that all sample 1 giants to the right of the CDL have $i_{\rm predict} < 2\overset{\circ}{.}0$. These extremely low

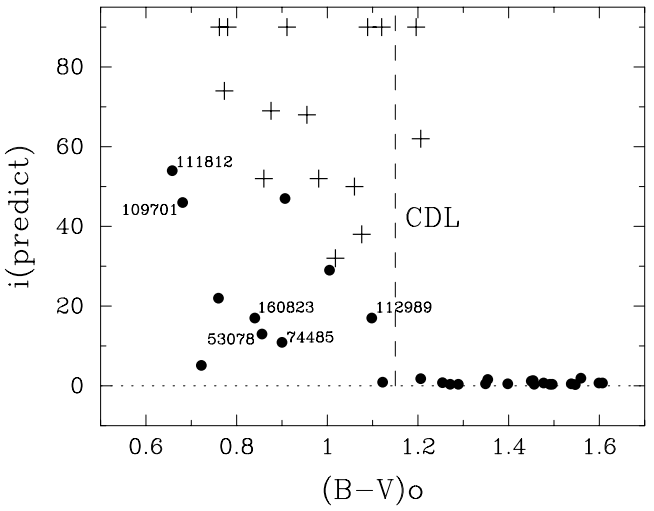

FIG. 8.—Predicted rotational inclinations in degrees, $i_{predict}$, plotted as filled circles, for the 29 giants in sample 1 that have variability timescales (Tables 1 and 5) as well as *Hipparcos* parallaxes. The approximate location of the CDL is indicated by the dashed line. Six of the eight variable giants labeled in Fig. 5 have variability timescales and are labeled with their HD numbers. The predicted inclinations of a sample of single, chromospherically active giants known to exhibit rotational modulation of starspots are plotted as pluses.

inclinations implied by the $i_{predict}$ values would make it impossible to observe rotational modulation. These contradictions demonstrate that rotational modulation cannot be the cause of variability in the giants to the right of the CDL.

The sample 1 giants (*filled circles*) on the left of the CDL in Figure 8 have significantly larger values of $i_{predict}$ than those on the right. This should be the case to some extent because of the systematically decreasing radius and slowly increasing mean $v \sin i$ with decreasing $(B-V)_0$ color. However, if rotational modulation is the mechanism of variability in these giants, then half of the values of $i_{predict}$ should be greater than 60°. This is clearly not the case; all values of $i_{predict}$ are *less* than 60°. Therefore, contrary to our earlier supposition, rotation is unlikely to be the cause of the observed variability in most of the giants to the left of the CDL.

It is possible, however, that rotational modulation is present in certain individual cases. Six of the eight chromospherically active variables in the upper left region of Figure 5 also appear in Figure 8 to the left of the CDL. Four of them, HD 53078, HD 74485, HD 112989, and HD 160823, have $i_{predict} \leq 20°$. We estimate the errors in $i_{predict}$, based on uncertainties in parallax, $v \sin i$, and the timescales of variability (each roughly 20%), to be in the range 30%–50%. Hence, none of these four giants, nor the other four giants to the left of the CDL with $i_{predict} < 30°$, are likely to be starspot variables (see note on HD 112989 in Appendix A).

Of the sample 1 giants in Figure 8 (*filled circles*) with $i_{predict} > 40°$, HD 109701 and HD 111812 are chromospherically active (from Fig. 5). The third star is HD 205603 and has $\log R'_{HK} = -4.93$, below the lower limit for enhanced chromospheric activity, so its variability mechanism is probably not rotational modulation of starspots. Considering the level of chromospheric activity and uncertainty in $i_{predict}$ for HD 109701 and HD 111812, rotational modulation is certainly a viable hypothesis for these two giants. This is strengthened by their rapid rotation, 9.9 and 57 km s^{-1}, respectively. Also, Strassmeier et al. (1994b) reported photospheric line-profile variability for HD 111812 and interpreted the changes as the result of rotational modulation.

Thus, the results of Figure 8, derived from 29 giants of sample 1 with computed values of $i_{predict}$, allow us to generalize our findings on rotational modulation to the larger sample of giants. Since all of the 18 sample 1 giants to the right of the CDL in Figure 8 have $i_{predict} < 2°$, rotational modulation can be ruled out as the cause of the observed photometric variations for all giants in the larger sample to the right of the CDL in Figure 3. Similarly, since only two of 11 giants to the left of the CDL in Figure 8 may have rotational modulation, this is not likely to be the variability mechanism for most giants to the left of the CDL in Figure 3.

This result is further strengthened by examining $i_{predict}$ values for a sample of single or effectively single, chromospherically active giants taken from Fekel & Balachandran (1993, 1994). From those two papers, we selected the 15 giants for which *Hipparcos* parallaxes as well as $v \sin i$ values and rotation periods are available in the literature. Photometric variability in these giants is the result of rotational modulation of starspots. We added our resulting $i_{predict}$ values to Figure 8 as plus symbols. Their distribution differs markedly from that of the sample 1 giants; a large fraction have $i_{predict} > 60°$, as expected for a sample of rotational variables.

Since rotational modulation cannot be the primary variability mechanism, we now consider evidence for pulsation in these giants. The mechanism for light variability in M giants is believed to be radial pulsation in the first or second overtone or perhaps the fundamental mode (e.g., Percy & Parkes 1998). To see if this mechanism extends to the G and K giants, we compare our observed timescales of photometric variability with pulsation periods computed from theoretical models.

In Table 7 we list the 29 giants from sample 1 that have both photometric variability timescales and *Hipparcos* parallaxes. The giants are tabulated in increasing $(B-V)_0$ order; column (1) gives the HD number and column (2) the $(B-V)_0$. Columns (3) and (4) list the mass and radius, respectively. Except in a few cases, we have estimated masses for the giants by comparing their effective temperatures and luminosities with the solar-abundance evolutionary tracks of Schaller et al. (1992). Our $(B-V)_0$ values were converted to effective temperatures with the relation of Flower (1996), and the luminosities (Table 1) were computed from the *Hipparcos* parallaxes. The mass of the very metal-poor giant HD 165195 was assumed to be 1.0 $M_\odot$, while a mass of 2.0 $M_\odot$ was used for HD 145895 and HD 215427, both of which have very small parallaxes with very large errors. Except for the latter two giants, the radii are from Table 1. For HD 145895 and HD 215427 radii were assumed from their spectral types and the results of Dumm & Schild (1998). We estimate a mass uncertainty of ≤ 0.5 $M_\odot$ for the eight giants in or near the Hertzsprung gap and an uncertainty of 1 $M_\odot$ for cooler giants. The vast majority of the radii have uncertainties of $\leq 15\%$. Column (5) gives three predicted radial pulsation periods for each giant: the fundamental mode, first overtone, and second overtone. These periods are computed with the formulae of Cox, King, & Stellingwerf (1972) and are a function of each star's

TABLE 7

COMPARISON OF PREDICTED RADIAL PULSATION PERIODS WITH OBSERVED TIMESCALES OF PHOTOMETRIC VARIABILITY

HD Number (1)	$(B-V)_0$ (mag) (2)	Mass ($M_\odot$) (3)	Radius ($R_\odot$) (4)	Predicted Period (days) (5)	Observed Timescale (days) (6)	Agreement with Theory[a] (7)
111812	0.658	2.6	9.7	0.7	7	No
				0.5		
				0.4		
109701	0.681	1.9	4.6	0.2	17	No
				0.2		
				0.1		
106270	0.722	1.4	2.9	0.1	5	No
				0.1		
				0.1		
29923	0.760	1.6	3.8	0.2	55	No
				0.1		
				0.1		
160823	0.840	3.0	15.6	1.3	25	No
				1.0		
				0.8		
53078	0.856	2.5	9.4	0.6	25	No
				0.5		
				0.4		
74485	0.900	2.8	12.3	0.9	25	No
				0.7		
				0.5		
205603	0.907	2.5	9.7	0.7	240	No
				0.5		
				0.4		
16761	1.005	2.0	8.7	0.6	120	No
				0.5		
				0.4		
112989	1.098	5.0	55.3	7.6	70	No
				5.5		
				4.2		
165195	1.122	1.0	32.8	10.6	10	Yes[b]
				5.9		
				3.9		
63838	1.206	1.5	13.9	1.6	15	No
				1.2		
				0.9		
120199	1.254	1.2	14.3	2.0	4	Yes:
				1.4		
				1.1		
109551	1.271	3.0	39.5	6.1	6	Yes
				4.3		
				3.2		
88748	1.289	3.0	41.4	6.6	6	Yes
				4.7		
				3.4		
109822	1.349	2.0	32.1	5.7	5	Yes
				4.0		
				2.8		
183909	1.354	3.0	48.0	8.6	10	Yes
				6.0		
				4.3		
112975	1.398	2.5	51.1	11.1	7	Yes
				7.3		
				5.1		
123232	1.450	3.0	71.0	17.5	12	Yes
				11.1		
				7.5		
215427	1.454	2.0	50.0	12.8	30	Yes:
				8.0		
				5.3		
155038	1.456	2.0	39.5	8.3	5	Yes
				5.5		
				3.8		

TABLE 7—*Continued*

HD Number (1)	$(B-V)_0$ (mag) (2)	Mass ($M_\odot$) (3)	Radius ($R_\odot$) (4)	Predicted Period (days) (5)	Observed Timescale (days) (6)	Agreement with Theory[a] (7)
84345	1.477	1.7	42.6	10.9	15	Yes:
				6.8		
				4.6		
175589	1.491	1.7	48.4	13.9	8	Yes
				8.3		
				5.5		
196643	1.496	2.0	53.9	14.8	7	Yes
				9.0		
				6.0		
3346	1.538	1.7	70.9	28.7	11	Yes
				14.6		
				9.4		
145895	1.547	2.0	50.0	12.8	10	Yes
				8.0		
				5.4		
208530	1.559	1.0	28.3	8.0	15	Yes:
				4.8		
				3.2		
200644	1.599	1.7	72.1	29.7	10	Yes
				14.9		
				9.7		
201298	1.607	1.7	72.3	29.8	12	Yes
				15.0		
				9.7		

[a] Yes: indicates agreement is only good to a factor of 2.
[b] Extreme metal-poor star for which the theoretical periods are not likely to be valid.

mass and radius. Increasing the mass decreases the predicted period, while increasing the radius increases it. Column (6) lists our timescales of photometric variability (Tables 1 or 5), which are mean values if two determinations were made. Column (7) indicates whether our timescales are compatible with the predicted pulsation periods.

Table 7 shows that the observed timescales of photometric variability are in agreement with predicted radial pulsation periods for all stars with $(B-V)_0 > 1.25$ mag. Most of the observed timescales for these stars are within the range of the predicted periods; four timescales are longer than the predicted fundamental period, but only by a factor of 2 at most. In contrast, all stars with $(B-V)_0 < 1.25$ mag, except for HD 165195, have predicted periods much shorter (by a factor of 10 or more) than the observed timescales. The star HD 165195 has an extremely low metallicity of $[Fe/H] = -2.25$. The theoretical pulsation models assume an extreme Population I composition (Cox et al. 1972), so the predicted periods for HD 165195 are not likely to be valid. These results argue that the radial pulsations found in M giants also occur in hotter giants with $(B-V)_0 > 1.25$ mag, i.e., up to spectral type K2–3 III, the approximate location of the coronal dividing line.

Additional evidence for radial pulsation in the giants on the cool side of the CDL comes from observed color changes. Table 8 compares mean ratios of the observed brightness changes in B to the observed changes in V for several classes of cool, giant variables that have been observed with the 0.4 m APT. These values correspond to slopes of the plotted ΔB versus ΔV data for each variable. The fourth column of the table gives the spread in the individual slopes within a variability type, computed as the standard deviation of an individual result from the mean in column (3). Since there is only one elliptical variable, its σ refers to the uncertainty in the single derived value of $\Delta B/\Delta V$. If $\langle \Delta B/\Delta V \rangle$ is equal to 1.0, then the star does not change color as it changes brightness. This kind of variability is seen in the elliptical variables, where brightness changes are caused primarily by viewing different aspects of a tidally distorted star. For $\langle \Delta B/\Delta V \rangle$ greater than 1.0, the amplitudes in B are greater than the amplitudes in V; i.e., the star becomes redder as it gets fainter. This is observed in the single and SB1 chromospherically active (CA) giants, where photometric variability is due to rotational modulation of cool, dark starspots. If $\langle \Delta B/\Delta V \rangle$ is less than 1.0, the star becomes bluer as it gets fainter. This occurs in semiregular variables, which are M giants similar to the Mira variables but with smaller amplitudes (typically 0.2–1.5 mag) and more irregular variations. Their variability is driven by radial p-mode pulsation. Seven of the K giants

TABLE 8

MEAN RATIOS OF PHOTOMETRIC $\Delta B/\Delta V$ FOR VARIOUS CLASSES OF COOL, GIANT VARIABLES OBSERVED WITH THE 0.40 m APT

Variable Type (1)	N_{stars} (2)	$\langle \Delta B/\Delta V \rangle$ (3)	σ (mag) (4)
Elliptical	1	0.98	0.03
Single CA giants	4	1.14	0.03
SB1 CA giants	8	1.12	0.03
Semiregular	5	0.92	0.04
K3–K5 giants	7	0.82	0.20
M0 giants	6	0.91	0.10

and six of the M giants from sample 1 that were reobserved with the 0.4 m APT (Table 5) and that have amplitudes sufficiently large to measure $\langle \Delta B/\Delta V \rangle$ are given as the last two entries in Table 8. The standard deviations for these two groups are considerably larger than for the other variable types, since their amplitudes are much smaller. It is clear, however, that the $\langle \Delta B/\Delta V \rangle$ values for both the K3–K5 and M0 giants agree with the mean value for the semiregular variables and not with the chromospherically active giants.

A final point concerns the shapes of the light curves of these giants on the cool side of the CDL. Although they have considerably smaller amplitudes, they look very similar to the light curves of typical M giant semiregular variables (e.g., Cristian et al. 1995).

We complete our discussion with a brief look at our results on the giants from samples 2 and 3, given in Tables 2 and 3, respectively.

Hall (1995) had compiled a list of 17 stars cataloged in the GCVS as K giant pulsating variables but hypothesized that they did not in fact comprise a class of variable stars. He predicted that these stars, upon closer inspection, would prove to be not K giants, not variable, or not pulsating. Improved spectral classification showed two (AW CVn and V538 Cas) are not K giants. Results for eight of the 17 stars are given in Table 2 and comprise our sample 2, the rest of Hall's sample being too faint or too far south to observe with our APTs in Arizona. For all of the stars in Table 2, our photometry failed to confirm the variability of large (0.9–1.2 mag) or even moderate (0.05–0.2 mag) amplitude given in the GCVS. Only four of the K giants in Table 2 are slightly variable ($\sigma_{\rm short} < 0.01$ mag). Three more are possibly variable, and one is constant. In conclusion, the stars cataloged in the GCVS as K giant pulsating variables do not, in a meaningful way, define a class of such variables. Either the spectral class proved wrong or the amplitude of variability proved spurious. Ironically, however, our photometry did find small-amplitude variability in several of the giants in this sample, in agreement with our results from sample 1, and so are likely to be low-amplitude pulsators.

We have found small-amplitude variability in the majority of giants in sample 3 (Table 3). These are (mostly K) giants for which Hatzes & Cochran (1998) find low-amplitude, radial velocity variations with both short and long periods. They concluded that the cause of the short-period variability is p-mode pulsation. They considered rotational modulation, planetary reflex motion, and g-mode pulsation as possible causes of the long-period variations. As in our sample 1 giants, we find very little evidence for periodicity in these sample 3 giants. In particular, we cannot confirm from our photometry any of the radial velocity periods reported by Hatzes & Cochran (1998). This is perhaps not too surprising since different radial velocity periods are sometimes found at different times in the same star (Tables 1 and 3 of Hatzes & Cochran 1998).

6. CONCLUSIONS

We find low-amplitude, short-term photometric variability in roughly one-fourth of our G giants, in half of the K giants, and in all of the M0 giants. The percentage of stars with variability is at a minimum for late G giants.

Rotational modulation of surface features cannot be the primary cause of photometric variability except, perhaps, for a few of the giants on the hot side of the CDL.

For giants on the cool side of the CDL, the variability mechanism is radial pulsation. Thus, the variability mechanism operating in M giants extends into the K giants up to about spectral class K2.

On the hot side of the CDL, timescales of photometric variability are incompatible with radial pulsation and, in most cases, rotation. Therefore, we conclude that the most likely variability mechanism in these stars is nonradial, g-mode pulsation.

Identification of the specific pulsation modes in these G and K giants will require further photometric and high-resolution spectroscopic observations and, especially, theoretical models with updated physics.

Many thanks go to Lou Boyd and Don Epand for their efforts at Fairborn Observatory. We also thank John Percy, Artie Hatzes, and the referee for useful comments on the paper. Astronomy with automated telescopes at Tennessee State University has been supported by the National Aeronautics and Space Administration, most recently through NASA grants NCC5-96 and NCC5-228 (which funds TSU's Center for Automated Space Science), and the National Science Foundation, most recently through NSF grant HRD-9706268 (which funds TSU's Center for Systems Science Research). This research has made use of the SIMBAD database, operated at CDS, Strasbourg, France.

APPENDIX A

NOTES ON SELECTED INDIVIDUAL STARS

Although not meant to be exhaustive, we made a literature search with SIMBAD for each giant. At the time of the search, over half of our 187 giants had two or fewer references listed. The following notes highlight additional aspects of some of the giants. We also provide comments based on our own observations. From a visual examination of our spectrograms, we have identified several moderately metal-poor or metal-rich giants.

A1. HD 3346 = HR 152

This M0 III is a spectroscopic binary with an orbital period of 576 days and an extremely small semiamplitude of 0.7 km s^{-1} (McClure et al. 1985). It is also a suspected variable, NSV 15135 (Kholopov 1982). Our photometric observations show a range of 0.05 mag in V with a timescale of 11 days, confirming the suspected light variability.

A2. HD 13611 = HR 649 = ξ^1 CET

This giant is a spectroscopic binary with a period of 1642 days and a possible white dwarf companion (Griffin & Herbig 1981). Griffin & Herbig (1981) noted the differing views concerning whether ξ^1 Cet is a mild barium star. Although Keenan &

Pitts (1980) classified it as a mild barium star, this anomaly was not noted in the later classification of Keenan & McNeil (1989), and Jorissen et al. (1998) have listed it as a normal giant with an orbit similar to those of barium stars.

HD 13611 is listed as suspected variable NSV 749 (Kholopov 1982). Our photometric observations show no light variations within each of three seasons. In fact, its value of $\sigma_{\rm short}$ is one of the lowest in our sample.

A3. HD 29139 = HR 1457 = α TAU = ALDEBERAN

Although we find α Tau, which is included in both samples 2 and 3, to be slightly variable based on its $\sigma_{\rm short}$ value of 0.0069 mag, we find no convincing evidence for periodicity between 0.1 and 200 days and so do not confirm the 92 day photometric period of Wasatonic & Guinan (1997). Our data set on α Tau is considerably longer than theirs and completely overlaps it in time. When we analyze only our data covering their time span, we still fail to find any convincing periodicity.

A4. HD 80811

Eggen (1997) listed HD 80811 as a member of the Arcturus group and gave a photometric abundance of [Fe/H] = −0.55. Our red wavelength spectrum confirms that the giant is metal-poor, and we estimate [Fe/H] = −0.6.

A5. HD 88547

The red wavelength spectrum of HD 88547 is similar to that of α Boo. Thus, we estimate [Fe/H] = −0.5.

A6. HD 88581

Comparison of the $B-V$ value corresponding to our spectral type with the *Hipparcos* $B-V$ (Perryman et al. 1997) suggests that HD 88581 has an early-type companion.

A7. HD 90127

From an objective prism spectrum Bidelman (1981) classified HD 90127 as a barium star. Lu (1991) estimated a Ba intensity of 2.0 and measured a radial velocity of −18 km s^{-1}. Our three velocities have a spread of 3.7 km s^{-1} over a range of 472 days, indicating that the giant is a long-period binary as expected from its barium star classification. Observations are continuing to determine its orbital elements.

A8. HD 91318

Comparison of the $B-V$ value corresponding to our spectral type with the *Hipparcos* $B-V$ (Perryman et al. 1997) suggests that HD 91318 has an early-type companion.

A9. HD 94177

Comparison of the $B-V$ value corresponding to our spectral type with the *Hipparcos* $B-V$ (Perryman et al. 1997) suggests that HD 94177 has an early-type companion.

A10. HD 109551 = HR 4795 = 6 DRA

Griffin, Eitter, & Reimers (1990) found this giant to be a spectroscopic binary with a period of 561.7 days and showed that it has a late A main-sequence companion.

A11. HD 111812 = HR 4883 = 31 COM

This star is a well-known, rapidly rotating, single giant in the Hertzsprung gap with spectral type G0 IIIp (Keenan & McNeil 1989) and $v \sin i = 57$ km s^{-1} (Strassmeier et al. 1994b). Although it has a very large Ca II H and K chromospheric flux (Strassmeier et al. 1990), no photometric variations have previously been found (Strassmeier & Hall 1988b). However, Strassmeier et al. (1994b) discovered absorption-line profile variations, which they suggested were most likely caused by cool starspots rotating into and out of view. Our photometric observations show that the giant has slight variability.

A12. HD 112989 = HR 4924 = 37 COM

In the first half of 1996 Strassmeier et al. (1997) observed this giant as a check star for 31 Com. They found HD 112989 to be variable with an amplitude of 0.02 mag in Strömgren y and suggested rotational modulation of starspots as the variability mechanism. From this 1996 season of data Strassmeier, Serkowitsch, & Granzer (1999) suggested a photometric period of around 80 days. During the following observing season they collected data over a 150 day interval but found no significant periodicity or light variability in those observations. Their spectra showed the giant to have weak Ca II H and K emission, and they estimated a low $v \sin i$ value of 4 ± 2 km s^{-1}.

De Medeiros, Konstantinova-Antova, & Da Silva (1999) recently obtained additional spectroscopic and photometric observations of HD 112989. They found it to be a single giant with Ca II H and K emission variability and, like Strassmeier et al. (1997), proposed that HD 112989 is a spotted star. Some of their results, however, differ significantly from those of Strassmeier et al. (1997, 1999). Instead of low-amplitude variability with a period of 2–3 months, their limited photometry during three seasons suggested 0.1–0.15 mag light variations over intervals of a few days. They also reported HD 112989 to be rapidly rotating with $v \sin i = 11.0 \pm 1.0$ km s^{-1}.

Our observations shed light on the sometimes conflicting results of the two groups. Our $v \sin i$ value of 12.0 ± 1.0 km s^{-1} is in excellent agreement with that given by De Medeiros et al. (1999) as is the mean of our two velocities listed in Table 9.

TABLE 9

INDIVIDUAL RADIAL VELOCITIES

HD Number	HJD − 2,400,000	Radial Velocity (km s^{-1})	Comment[a]
1594	51,003.981	4.6	
3346	51,089.864	−34.6	
3690	51,089.869	−18.7	
7681	50,635.959	−29.3	
10222	50,757.889	22.3	
11326	49,972.020	−57.3	
12252	50,362.887	14.6	
16761	51,089.937	21.8	
18474	51,089.945	6.2	
18832	50,757.898	−53.6	
19845	51,091.853	−11.0	
21585	50,362.919	34.0	
22695	50,363.904	15.2	
29923	49,973.953	20.5	
38229	50,364.930	17.3	
40458	50,365.950	−24.2	
41479	50,365.957	2.0	
	50,401.899	1.8	
41599	50,365.967	46.6	
41790	50,757.004	−3.8	
42596	50,757.014	32.3	
43299	51,089.997	−37.3	
47335	50,365.975	−17.0	
48270	50,365.980	20.5	
53078	50,363.998	−7.0	
	51,305.646	−7.7	Ca
	51,306.628	−6.7	
55969	50,401.927	−15.7	
	50,578.629	−15.9	
56245	50,401.949	−16.6	
	50,578.639	−17.1	
	50,927.651	−17.1	
61107	50,829.827	9.5	
	50,830.850	9.0	
63838	51,093.035	12.6	
66285	51,305.675	1.0	Ca
67541	50,756.974	−13.2	
68612	50,756.985	15.9	Variable velocity
	50,927.665	18.3	
	51,306.639	19.4	
70136	50,576.619	38.4	
	50,930.629	38.8	Ca
73799	50,830.912	25.2	Variable velocity
	50,930.650	22.0	Ca
74485	50,576.647	−13.1	
	51,305.706	−13.6	Ca
75216	50,576.640	−8.9	
76219	50,832.876	16.0	
	50,833.885	16.4	
	50,927.678	16.6	
80811	50,831.978	29.6	
84345	50,575.685	17.5	
84453	50,830.918	−44.2	
	50,930.709	−44.0	Ca
86166	50,831.990	1.4	
	50,832.825	1.3	
86873	50,831.998	−40.4	
	50,832.857	−40.5	
87210	50,832.008	24.7	
	50,832.867	24.6	
87623	50,832.023	62.0	
88476	50,832.900	4.1	
88547	50,832.881	32.0	
88581	50,830.999	7.2	

TABLE 9—*Continued*

HD Number	HJD − 2,400,000	Radial Velocity (km s^{-1})	Comment[a]
88748.....	50,575.703	−5.3	Variable velocity
	50,930.676	0.9	Ca
	51,303.758	−2.0	
89557.....	50,830.973	28.7	
	50,928.715	29.2	
89993.....	50,830.968	−14.2	
	50,930.693	−14.2	Ca
90127.....	50,831.011	−15.1	Variable velocity
	50,927.691	−16.7	
	51,303.779	−18.8	
90507.....	50,199.712	−4.6	
90990.....	50,631.634	−15.7	
91286.....	50,631.644	−33.4	
91318.....	50,832.926	13.0	
91684.....	50,832.945	25.5	
94177.....	50,198.776	12.5	Variable velocity
	50,930.770	10.3	Ca
	51,303.795	6.3	
94425.....	50,198.791	10.3	
104130	50,575.720	13.9	
	50,930.731	13.4	Ca
105089	50,831.015	16.6	
	50,927.709	17.2	
	50,930.748	17.0	Ca
105264	50,575.727	−11.9	
106270	50,833.975	24.2	
	51,305.737	24.7	Ca
107485	50,928.801	−11.5	
108973	50,928.783	4.2	
109551	50,575.730	11.7	Variable velocity
	50,577.846	12.6	Ca
	50,927.721	−0.3	
109701	50,575.746	−22.0	
	50,634.661	−21.3	Ca
109822	50,575.735	−31.7	
	50,578.848	−31.4	Ca
111812	51,305.767	6.8	Ca
112975	50,575.803	6.6	Possibly variable velocity
	50,634.661	8.1	Ca
	51,306.707	8.1	
	51,350.681	8.1	
112989	50,927.730	−14.5	
	50,930.786	−13.9	Ca
113253	50,833.911	−46.1	Variable velocity
	50,931.787	−41.7	
	51,303.882	−43.7	
113983	50,833.925	−4.7	
	51,305.789	−4.5	Ca
114417	51,005.692	−0.3	
114946	50,927.737	−47.8	
117304	50,927.742	1.0	
119826	50,831.025	−2.5	
120199	50,575.835	0.0	
	50,634.697	0.6	Ca
120602	50,576.780	−24.8	
	50,930.794	−24.3	Ca
121107	48,345.827	−10.9	
	48,348.779	−11.9	
	48,426.648	−11.7	
	48,771.783	−12.0	
	48,772.672	−11.9	
	50,263.626	−12.7	
	51,305.819	−11.0	Ca
122548	50,576.787	19.8	

TABLE 9—*Continued*

HD Number	HJD − 2,400,000	Radial Velocity (km s^{-1})	Comment[a]
122834	50,830.067	−3.5	
	50,928.877	−2.7	
	50,930.806	−2.7	Ca
123232	50,576.800	−12.0	Possibly variable velocity
	50,635.715	−10.0	Ca
124117	50,830.073	−26.4	
124572	50,830.079	1.2	
	50,928.895	0.4	
125711	51,005.707	−28.8	
128200	50,928.749	2.8	
128461	50,928.767	−14.9	
140716	51,004.814	−5.4	
143209	50,720.581	−16.1	
	50,930.841	−16.1	Ca
144015	50,576.811	−15.0	
	50,928.907	−14.5	
145004	50,720.588	23.2	
	50,930.865	22.8	Ca
	50,931.878	23.3	
145894	50,720.596	−23.6	
145895	50,576.823	−6.8	
	50,634.744	−5.9	Ca
145957	50,576.829	−13.1	
	50,577.759	−13.1	
	50,577.881	−13.7	Ca
	50,636.774	−13.0	
150050	50,198.930	8.1	
	50,930.887	7.8	Ca
	50,931.889	8.1	
154815	50,630.874	−38.1	
155028	51,004.750	14.5	
155038	50,362.592	−2.5	
	50,578.878	−2.6	Ca
155136	50,630.882	−11.3	
155526	50,631.769	−10.5	
156296	50,720.606	−49.6	
156910	50,720.615	−34.7	
157911	50,630.890	−35.9	
	50,931.897	−36.3	
159544	50,630.900	−59.0	
	50,930.916	−60.1	Ca
	50,931.908	−59.5	
159887	50,718.656	5.9	
160385	50,362.600	26.9	
	50,930.942	26.3	Ca
160507	50,718.668	−12.0	
160823	50,199.937	−6.9	Variable velocity
	51,305.877	0.4	Ca
165195	50,577.937	−1.7	Ca, Probably variable velocity
	50,630.913	0.8	
	51,004.770	−0.9	
	51,307.896	−0.2	Li
	51,350.841	−0.1	
166284	50,718.676	−58.4	
166460	50,719.685	6.3	
166955	50,630.925	6.9	
167587	50,719.695	−10.0	Variable velocity
	50,931.935	−11.4	
	51,308.849	−15.8	
	51,351.841	−16.3	
168619	50,719.709	6.0	
175589	50,362.654	−14.6	
	50,578.911	−15.1	Ca
177251	50,719.722	12.3	
	51,305.940	11.7	Ca

TABLE 9—*Continued*

HD Number	HJD − 2,400,000	Radial Velocity (km s^{-1})	Comment[a]
177370	50,362.666	1.5	
	50,634.793	1.2	Ca
181380	50,630.934	−11.0	
182567	50,720.729	−60.6	
182896	50,630.942	−17.4	
183387	50,930.954	−61.1	Ca
	50,931.984	−60.4	
183909	50,362.677	18.4	
	50,577.965	18.0	Ca
185018	51,089.700	−0.9	
	51,305.966	−0.9	Ca
188256	50,757.621	−23.2	
189533	51,089.707	−3.6	
190940	50,930.963	−10.0	Ca
	50,932.014	−9.8	
192274	50,719.772	−38.3	
	50,930.975	−38.6	Ca
192800	50,719.785	−51.3	
196229	50,362.683	18.9	Possibly variable velocity
	50,578.936	16.8	Ca
	50,636.831	18.5	
	51,349.939	18.4	
196642	50,756.549	−37.7	
	51,305.982	−38.1	Ca
196643	50,362.691	−9.4	
	50,578.962	−11.1	Ca
	51,349.934	−10.1	
196688	50,756.635	−6.0	
	50,931.990	−6.2	
197274	50,203.945	12.8	
197644	50,203.955	16.9	
200413	50,266.987	−19.6	
200497	51,003.937	1.5	
200577	51,003.938	−4.3	
200644	50,361.755	−16.0	
	50,578.988	−16.4	Ca
201053	50,756.625	−79.1	
	50,932.004	−78.9	
201298	50,361.758	17.2	
	50,930.993	18.0	Ca
202573	49,968.860	−25.9	
202975	51,003.944	13.8	
203344	51,003.949	−88.2	
	51,089.716	−88.3	
205603	50,931.005	−5.9	Ca
	50,931.998	−5.8	
208530	50,361.767	7.8	
209396	51,003.954	39.5	
209408	50,753.720	13.2	
210269	51,003.961	−45.7	
	51,089.723	−45.7	
215427	49,968.826	−18.7	
216143	50,753.703	−116.4	

[a] Ca: 3950 Å region; Li: 6700 Å region.

However, similar to the results of Strassmeier et al. (1997), our four seasons of photometry show a maximum amplitude of about 0.03 mag and a variability timescale of 70 days (Fig. 6). Our single observation of the 3950 Å region indicates that HD 112989 has very weak Ca II H and K emission lines. In fact, its emission flux (Fig. 5) is just above the threshold used to identify chromospherically active binaries (Strassmeier et al. 1993). As noted in our discussion section, the low predicted rotational inclination of 17° argues *against* rotational modulation of starspots as the cause of light variability in HD 112989.

A13. HD 113983

Abt (1984) classified this giant as G8 IIIp (Ca II weak). The *Hipparcos* value of $B-V$ is 0.15 mag bluer than the $B-V$ corresponding to our spectral type of G7 III, suggesting that HD 113983 has an early-type companion.

A14. HD 121107 = HR 5225 = 7 BOO

This star is a rapidly rotating, single giant in the Hertzsprung gap. Strassmeier et al. (1994a) found its chromospheric flux to be at the lower end of the range found for active chromosphere stars. Our photometric observations show slight variability.

A15. HD 128461

On the basis of Strömgren four-color photometry, Olsen (1979) predicted that HD 128461 might have a composite spectrum. Comparison of the $B-V$ value corresponding to our spectral type with the *Hipparcos* $B-V$ (Perryman et al. 1997) suggests that HD 128461 has an early-type companion.

A16. HD 159544

Although the mean radial velocity of HD 159544 is quite large, -59.5 km s^{-1}, the star appears to be *metal-rich*, with [Fe/H] ~ 0.3.

A17. HD 160507 = HR 6579

From an objective prism spectrum, Bidelman (1985) classified this giant as a barium star.

A18. HD 160823

Harlan (1974) classified HD 160823 as G2 II while Keenan & McNeil (1989) found G0: IIIa, both of which are in good agreement with our result of G1 II:.

A19. HD 165195

Morgan described the spectrum of HD 165195 as very peculiar (Wallerstein et al. 1963), and the spectroscopic abundance study of Wallerstein et al. (1963) showed it to be an extremely metal-poor giant. A more recent spectroscopic analysis by Sneden & Crocker (1988) found [Fe/H] $= -2.25$.

From five spectrograms, Wallerstein et al. (1963) reported a mean radial velocity of -0.2 km s^{-1} and called the velocity definitely constant. Our mean velocity of -0.5 km s^{-1} is in excellent agreement with that result. However, our velocity range of 2.5 km s^{-1} suggests that the giant may have low-amplitude velocity variations.

Dupree & Smith (1995) obtained five echelle spectra of its Ca II K line over a period of 8 yr. The Ca II K emission feature showed significant changes in its strength, asymmetry, and width. Dupree & Smith (1995) concluded that the variability of the Ca II K emission line indicates that, in deep regions of the chromosphere, inflow and outflow are occurring at modest speeds, possibly driven by pulsation.

Our photometry of this very metal-poor giant shows it to be variable with a maximum amplitude of 0.04 mag in V and a timescale of 10 days (Fig. 7).

A20. HD 168619

The red wavelength spectrum of HD 168619 indicates that it is somewhat metal-poor, and we estimate [Fe/H] $= -0.4$ from comparison with various spectral-type standards.

A21. HD 182567

The red wavelength spectrum of HD 182567 is similar to that of α Boo. Thus, we estimate [Fe/H] $= -0.5$.

A22. HD 201053

The mean velocity of HD 201053 is -79.0 km s^{-1}, making this giant a high-velocity star based on its radial velocity alone.

A23. HD 203344 = HR 8165 = 34 VUL

The mean velocity of HD 203344 is -88.2 km s^{-1}, making this giant a high-velocity star based on its radial velocity alone.

A24. HD 216143

This star is a very metal-poor giant for which Luck & Bond (1981) determined a spectroscopic [Fe/H] value of -2.27. Unlike HD 165195, it is a high-velocity giant having a radial velocity of -116.4 km s^{-1}. Smith & Dupree (1998) examined the Hα and Ca II K lines and found no evidence of chromospheric outflow from those lines. However, the Mg II h and k emission features showed profiles characteristic of mass outflow from the chromosphere.

APPENDIX B

INDIVIDUAL RADIAL VELOCITIES

Table 9 in this appendix lists our individual radial velocities computed from red wavelength spectra for 147 giants. Forty-eight giants have radial velocities computed from blue wavelength spectra. A total of 66 stars have more than one measurement. Column (1) identifies each giant by its HD number. Columns (2) and (3) give the heliocentric Julian date of the

observation and the measured radial velocity. Column (4) identifies the wavelength region if it is not 6430 Å and notes stars that have velocity variability.

The radial velocities were measured with the KPNO IRAF cross-correlation program FXCOR (Fitzpatrick 1993). Several IAU velocity standards (Pearce 1957) were observed during the course of each night, and their velocities adopted from the work of Scarfe, Batten, & Fletcher (1990). For the red wavelength spectra, the region used for the correlation was 6404–6444 Å, which is relatively insensitive to spectral-type mismatch between the standard and program star. Those velocities have typical uncertainties of ≤ 0.5 km s^{-1}. Blue wavelength spectra of the Ca II H and K region were obtained for 48 giants. Those radial velocities were measured by cross-correlating part of the region between the K and H lines, 3945–3960 Å. Velocity uncertainties of the blue wavelength spectra are estimated to be ≤ 1.0 km s^{-1}.

REFERENCES

Abt, H. A. 1984, ApJ, 285, 247
Baliunas, S. L., Donahue, R. A., Soon, W., & Henry, G. W. 1998, in ASP Conf. Ser. 154, Cool Stars, Stellar Systems, and the Sun, ed. R. A. Donahue & J. A. Bookbinder (San Francisco: ASP), 153
Bidelman, W. P. 1981, AJ, 86, 553
———. 1985, AJ, 90, 341
Choi, H.-J., Soon, W., Donahue, R. A., Baliunas, S. L., & Henry, G. W. 1995, PASP, 107, 744
Cox, J. P., King, D. S., & Stellingwerf, R. F. 1972, ApJ, 171, 93
Cristian, V. C., Donahue, R. A., Soon, W. H., Baliunas, S. L., & Henry, G. W. 1995, PASP, 107, 411
Cummings, I. N., Hearnshaw, J. B., Kilmartin, P. M., & Gilmore, A. C. 1999, in ASP Conf. Ser. 185, Precise Stellar Radial Velocities, ed. J. B. Hearnshaw & C. D. Scarfe (San Francisco: ASP), 204
De Medeiros, J.-R., Da Rocha, C., & Mayor, M. 1996, A&A, 314, 499
De Medeiros, J.-R., Konstantinova-Antova, R. K., & Da Silva, J. R. P. 1999, A&A, 347, 550
Dumm, T., & Schild, H. 1998, NewA, 3, 137
Dupree, A. K., & Smith, G. H. 1995, AJ, 110, 405
Eaton, J. A., Boyd, L. J., & Henry, G. W. 1996, BAAS, 28, 841
Edmonds, P. D., & Gilliland, R. L. 1996, ApJ, 464, L157
Eggen, O. J. 1997, AJ, 114, 825
Eyer, L., Grenon, M., Falin, J.-L., Froeschlé, M., & Mignard, F. 1994, Sol. Phys., 152, 91
Fekel, F. C. 1997, PASP, 109, 514
Fekel, F. C., & Balachandran, S. 1993, ApJ, 403, 708
———. 1994, in ASP Conf. Ser. 64, Cool Stars, Stellar Systems, and the Sun, ed. J.-P. Caillault (San Francisco: ASP), 279
Fekel, F. C., & Henry, G. W. 1998, in ASP Conf. Ser. 154, Cool Stars, Stellar Systems, and the Sun, ed. R. A. Donahue & J. A. Bookbinder (San Francisco: ASP), 755
FitzGerald, M. P. 1970, A&A, 4, 234
Fitzpatrick, M. J. 1993, in ASP Conf. Ser. 52, Astronomical Data Analysis Software and Systems II, ed. R. J. Hanish, R. V. J. Brissenden, & J. Barnes (San Francisco: ASP), 472
Flower, P. J. 1996, ApJ, 469, 355
Gautschy, A., & Saio, H. 1996, ARA&A, 34, 551
Griffin, R. F., Eitter, J. J., & Reimers, D. 1990, J. Astrophys. Astron., 11, 255
Griffin, R. F., & Herbig, G. H. 1981, MNRAS, 196, 33
Haisch, B. M. 1999, in The Many Faces of the Sun, ed. K. T. Strong, J. L. R. Saba, B. M. Haisch, & J. T. Schmelz (New York: Springer), 481
Hall, D. S. 1995, in ASP Conf. Ser. 79, Robotic Telescopes: Current Capabilities, Present Developments, and Future Prospects for Automated Astronomy, ed. G. W. Henry & J. A. Eaton (San Francisco: ASP), 65
Harlan, E. A. 1974, AJ, 79, 682
Hatzes, A. P., & Cochran, W. D. 1993, ApJ, 413, 339
———. 1994a, ApJ, 422, 366
———. 1994b, ApJ, 432, 763
———. 1998, in ASP Conf. Ser. 154, Cool Stars, Stellar Systems, and the Sun, ed. R. A. Donahue & J. A. Bookbinder (San Francisco: ASP), 311
Henry, G. W. 1995a, in ASP Conf. Ser. 79, Robotic Telescopes: Current Capabilities, Present Developments, and Future Prospects for Automated Astronomy, ed. G. W. Henry & J. A. Eaton (San Francisco: ASP), 37
———. 1995b, in ASP Conf. Ser. 79, Robotic Telescopes: Current Capabilities, Present Developments, and Future Prospects for Automated Astronomy, ed. G. W. Henry & J. A. Eaton (San Francisco: ASP), 44
———. 1999, PASP, 111, 845
Henry, G. W., Eaton, J. A., Hamer, J., & Hall, D. S. 1995a, ApJS, 97, 513
Henry, G. W., Fekel, F. C., & Hall, D. S. 1995b, AJ, 110, 2926
Hoffleit, D., & Jaschek, C. 1982, The Bright Star Catalogue (4th ed.; New Haven: Yale Univ. Obs.)
Johnson, H. L. 1966, ARA&A, 4, 193
Jorissen, A., Mowlavi, N., Sterken, C., & Manfroid, J. 1997, A&A, 324, 578
Jorissen, A., Van Eck, S., Mayor, M., & Udry, S. 1998, A&A, 332, 877
Keenan, P. C., & McNeil, R. C. 1989, ApJS, 71, 245
Keenan, P. C., & Pitts, R. E. 1980, ApJS, 42, 541
Kholopov, P. N. 1982, New Catalogue of Suspected Variable Stars (Moscow: Nauka)
———. 1985, General Catalogue of Variable Stars (Moscow: Nauka)
Larson, A. M., Yang, S. L. S., & Walker, G. A. H. 1999, in ASP Conf. Ser. 185, Precise Stellar Radial Velocities, ed. J. B. Hearnshaw & C. D. Scarfe (San Francisco: ASP), 193
Linsky, J. L., Worden, S. P., McClintock, W., & Robertson, R. M. 1979, ApJS, 41, 47
Lockwood, G. W., Skiff, B. A., & Radick, R. R. 1997, ApJ, 485, 789
Lu, P. K. 1991, AJ, 101, 2229
Luck, R. E., & Bond, H. E. 1981, ApJ, 244, 919
McClure, R. D., Griffin, R. F., Fletcher, J. M., Harris, H. C., & Mayor, M. 1985, PASP, 97, 740
Noyes, R. W., et al. 1984, ApJ, 279, 763
Olsen, E. 1979, A&AS, 37, 367
Pearce, J. A. 1957, Trans. IAU, 9, 441
Percy, J. R. 1993, PASP, 105, 1422
Percy, J. R., & Parkes, M. 1998, PASP, 110, 1431
Perryman, M. A. C., et al. 1997, The *Hipparcos* and Tycho Catalogues (ESA-SP 1200; Noordwijk: ESA)
Russell, H. N., Dugan, R. S., & Stewart, J. Q. 1938, Astronomy II. Astrophysics & Stellar Astronomy (Boston: Ginn & Co.), 701
Scarfe, C. D., Batten, A. H., & Fletcher, J. M. 1990, Publ. Dom. Astrophys. Obs. Victoria, 18, 21
Schaller, G., Schaerer, D., Meynet, G., & Maeder, A. 1992, A&AS, 96, 269
Smith, G. H., & Dupree, A. K. 1998, AJ, 116, 931
Smith, P. H., McMillan, R. S., & Merline, W. J. 1987, ApJ, 317, L79
Sneden, C. A., & Crocker, D. A. 1988, ApJ, 335, 406
Strassmeier, K. G., Boyd, L. J., Epand, D. H., & Granzer, Th. 1997, PASP, 109, 697
Strassmeier, K. G., & Fekel, F. C. 1990, A&A, 230, 389
Strassmeier, K. G., Fekel, F. C., Bopp, B. W., Dempsey, R. C., & Henry, G. W. 1990, ApJS, 72, 191
Strassmeier, K. G., & Hall, D. S. 1988a, ApJS, 67, 453
———. 1988b, ApJS, 67, 439
Strassmeier, K. G., Hall, D. S., Boyd, L. J., & Genet, R. M. 1989, ApJS, 69, 141
Strassmeier, K. G., Hall, D. S., Fekel, F. C., & Scheck, M. 1993, A&AS, 100, 173
Strassmeier, K. G., Handler, G., Paunzen, E., & Rauth, M. 1994a, A&A, 281, 855
Strassmeier, K. G., Serkowitsch, E., & Granzer, Th. 1999, A&AS, 140, 29
Strassmeier, K. G., Washüttl, A., & Rice, J. B. 1994b, Inf. Bull. Variable Stars, 3994, 1
Walker, G. A. H., Yang, S., Campbell, B., & Irwin, A. W. 1989, ApJ, 343, L21
Wallerstein, G., Greenstein, J. L., Parker, R., Helfer, H. L., & Aller, L. H. 1963, ApJ, 137, 280
Wasatonic, R., & Guinan, E. F. 1997, Inf. Bull. Variable Stars, 4480, 1